EVOLUTION OF REGIONAL STRESS STATE BASED ON FAULTING AND FOLDING NEAR THE PIT RIVER, SHASTA COUNTY, CALIFORNIA

by

LAUREN JEAN AUSTIN

A THESIS

Presented to the Department of Geological Sciences
and the Graduate School of the University of Oregon
in partial fulfillment of the requirements
for the degree of
Master of Science

September 2013

THESIS APPROVAL PAGE

Student: Lauren Jean Austin

Title: Evolution of Regional Stress State Based on Faulting and Folding Near the Pit River, Shasta County, California

This thesis has been accepted and approved in partial fulfillment of the requirements for the Master of Science degree in the Department of Geological Sciences by:

Ray J. Weldon	Chairperson
Joshua J. Roering	Member
Marli B. Miller	Member

and

Kimberly Andrews Espy	Vice President for Research and Innovation; Dean of the Graduate School

Original approval signatures are on file with the University of Oregon Graduate School.

Degree awarded September 2013

THESIS ABSTRACT

Lauren Jean Austin

Master of Science

Department of Geological Sciences

September 2013

Title: Evolution of Regional Stress State Based on Faulting and Folding Near the Pit River, Shasta County, California

We investigate the evolution of the regional stress state near the Pit River, northern California, in order to understand the faulting style in a tectonic transition zone and to inform the hazard analysis of Fault 3432 near the Pit 3 Dam. By analyzing faults and folds preserved in and adjacent to a diatomite mine north of the Pit River, we have determined principal stress directions preserved during the past million years. We find that the stress state has evolved from predominantly normal to strike slip and most recently to reverse, which is consistent with regional structures such as the extensional Hat Creek Fault to the south and the compressional folding of Mushroom Rock to the north. South of the Pit River, we still observe normal and strike slip faults, suggesting that changes in stress state are moving from north to south through time.

CURRICULUM VITAE

NAME OF AUTHOR: Lauren Jean Austin

GRADUATE AND UNDERGRADUATE SCHOOLS ATTENDED:

University of Oregon, Eugene
University of California, Davis
University of Washington, Seattle

DEGREES AWARDED:

Master of Science, Geology, 2013, University of Oregon
Bachelor of Science, Geology, 2011, University of California, Davis

AREAS OF SPECIAL INTEREST:

Neotectonics/Quaternary geology
Geomorphology

PROFESSIONAL EXPERIENCE:

Research assistant, University of Oregon, 2011-2013

Lab assistant, Stable isotopes lab, UC Davis, 2009-2011

GRANTS, AWARDS, AND HONORS:

Graduate Teaching Fellowship, University of Oregon, 2011-2013

NSF SIGNS Scholarship, UC Davis, 2010

PUBLICATIONS:

Weldon, R.J., Schmidt, D.A., **Austin, L.J.,** Weldon, E.M., Dawson, T.E., 2013. Appendix D-Compilation of Creep Rate Data for California Faults and Circulation of Moment Reduction Due to Creep *in* Uniform California Earthquake Rupture Forecast Version 3, USGS Open File Report 2013-65D and California Geological Survey Special Report 228D. 43 pages.

Austin, L.J., Weldon, R.J., and Paulson, K.T., 2012. Distribution of Faults in a Transition zone: Multimodal Faulting in the Pit River region, Shasta County, CA, Abstract T33F-2717 presented at the 2012 Fall Meeting, AGU, San Francisco, CA, 3-7 Dec.

Austin, L.J., Roeske, S., Garber, J., Wimpenny, J., Yin, Q., 2011. Detrital Zircon Geochronology of Lower to Mid-Crustal Rocks Associated with a Microplate-Continent Collision, NW Argentina. Abstract T51A-2317 presented at the 2011 Fall Meeting, AGU, San Francisco, CA, 5-9 Dec.

ACKNOWLEDGMENTS

I extend my thanks to my thesis committee, Josh Roering, Marli Miller, and especially my advisor, Ray Weldon, who treated me like a colleague, listened to my ideas, and taught me how to have a scientific dialogue. I owe sincere thanks to Bill Page and PG&E for funding this project and being helpful and supportive throughout the entire process. In addition, I greatly appreciate Dicalite Minerals Corp., particularly Rocky Torgrimson and Paul Budesa, for their generous help and enthusiastic interest in my project while I was working in their mine. This project would not have been possible without their consent and assistance. I am grateful for the hospitality of Rocky and Becky Torgrimson during my stay in Burney.

Ray and LiLi Weldon, Jessica Vigil, Colby Munson, Katie Paulson, and Jo Byrnes provided excellent and enthusiastic help in the field. I appreciate valuable field discussions with Tom Sawyer, Dylan Rood, Seth Dee, Simon Kattenhorn, Matt Blakeslee, and others, which served to deepen my understanding of the regional geology and structure.

I would also like to thank my fellow UO geology graduate students for their constant support, and in particular Ashley Streig for teaching me how to use software programs, write abstracts, and believe in my abilities. My deepest thanks goes to my family and their unconditional love and support.

This project was funded by a gift from Pacific Gas and Electric, and by the University of Oregon Department of Geological Sciences.

TABLE OF CONTENTS

LIST OF FIGURES

LIST OF TABLES

CHAPTER I

INTRODUCTION

1. Overview

For this project, I investigated surface deformation – faults and folds – in the Pit River region of northern California to determine the regional stress state and help inform the hazard analysis of the Pit 3 Dam. In Chapter I, I describe the tectonic setting of the study area and explain the motivation for the project. In Chapter II, I explain the techniques I used in the field and in subsequent analysis of field data; in Chapter III I present the results from data analysis and show the probable progression of regional stresses. I discuss the structural and regional implications of these results in Chapter IV.

2. Tectonic setting

The Pit River region of northern California is situated in a transition zone between several significant volcanic and tectonic provinces (Figure 1). Generally east-west convergence of the Gorda and North American plates results in subduction of the Gorda plate beneath North America. The resulting arc volcanism reaches as far south as the intermediate and mixed volcanics of California's Mount Shasta and Lassen Peak, which bracket the Pit River region to the north and south, respectively (Figure 1). West of the arc, east-west to north-south shortening occurs within the Klamath Mountains region. East of the arc, extensional faulting and voluminous basaltic volcanism of the Modoc Plateau make up the northwestern corner of the Basin and Range extensional province (White and Crider, 2006). The Basin and Range, and to a lesser extent the Modoc Plateau, is characterized by east-west extension that produces north- to northeast-striking normal faulting and distinctive horst and graben topography. To the south, interactions

between the Pacific and the North American plates dominate the tectonics. The dextral San Andreas Fault accommodates much of the relative plate motion, but 15-25% of the total motion is accommodated in the western Great Basin, and specifically in the Walker Lane east of the Sierra Nevada (Figure 1; Faulds, 2005).

The Sierra Nevada Mountains and the adjacent Great Valley to the west together behave as a rigid block, with regional deformation occurring on the margins between the Sierra Nevada-Great Valley block and neighboring provinces (McCaffrey, 2005). Because deformation is concentrated on the well-developed San Andreas Fault margin, dextral shear occurs at a faster rate on the west side of the Sierra Nevada-Great Valley block than on the east. This distribution of dextral motion results in the entire Sierra Nevada-Great Valley block being translated northward, causing compression in the Klamath Mountains and contributing to the clockwise rotation of the Oregon forearc where the Sierran microplate and the Cascadia forearc blocks meet (McCaffrey, 2007). GPS measurements of strain have been particularly useful in resolving strain distribution related to plate boundary motion. Geodetic measurements show that slip is concentrated in the diffuse but discrete zone of Walker Lane east of the rigid Sierran microplate and provides high resolution strain rates (Hammond, 2005; McCaffrey, 2007). Some of the Walker Lane shear propagates northwestward across northern California, appearing to pass through the Pit River region, and appears to connect with the poorly defined zones of deformation between the Gorda, Pacific, and North American plates near the Klamath Mountains (Miller, 2001). Modern GPS data show strain rates of ~11 mm/yr across Walker Lane, compatible with rates determined by very long baseline interferometry (VLBI) and integrated net shear methods based on geologic data (Dokka, 1990; Argus,

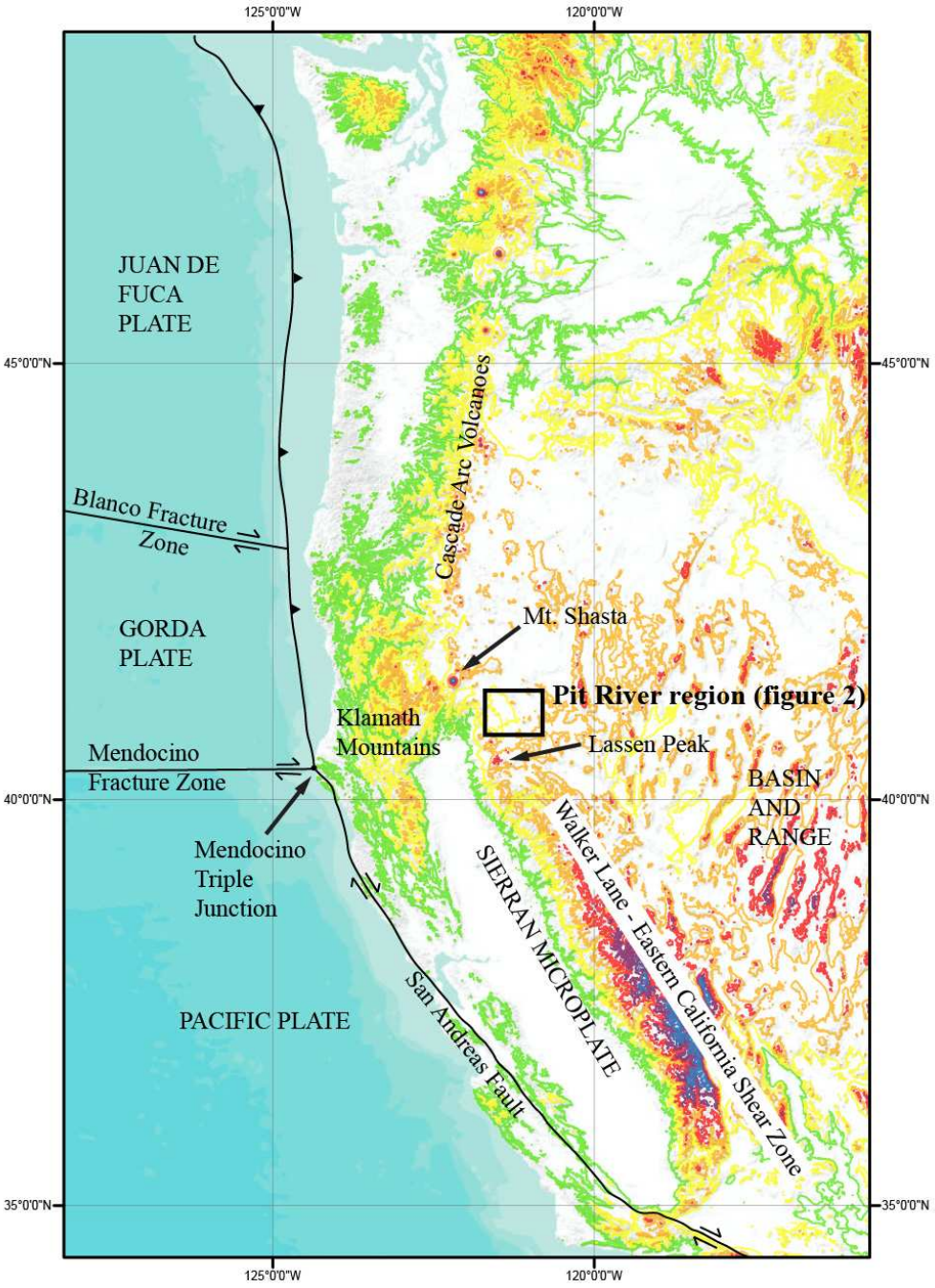

Figure 1. The greater tectonic setting of the Pit River region - the western US - is a complex zone of plate boundaries and interactions. Convergence of the Juan de Fuca and Gorda plates with the North American plate form the Cascadia subduction zone and associated Cascade arc volcanism; the Pit River is just north of the southernmost Cascade arc volcano, Lassen Peak. The transform boundary between the Pacific and North American plates includes the dextral San Andreas fault and associated structures. The Walker Lane zone of diffuse dextral shear separates the extensional Basin and Range from the Sierran microplate and projects northward into the Pit River region. The Sierran microplate pushes northward like a piston into northern California and southern Oregon.

1991; Sauber, 1994; Bennett, 1999; Dixon, 2000; Hammond, 2007). Strain accommodated in Walker Lane appears to be in the process of consolidating onto a smaller number of dominant structures in the southeast and is more diffuse as it propagates to the northwest (Hammond, 2007). The Pit River region experiences some of this diffuse dextral shear related to Pacific-North American plate motion. Specifically, at the boundary between the southern end of the Cascade Range block and the northern edge of Walker Lane, dextral shear is transferred to the west, which results in Quaternary compression in the northern Central Valley. The Inks Creek Fold Belt is an example of this recent shortening (Sawyer, 2010), as well as the proposed Mushroom Rock anticline (Sawyer, 2011).

Crustal stresses related to these complex block motions and volcanic processes drive regional seismicity and form the observed patterns of faulting around the Pit River. Sequences of earthquakes near Lassen Peak and Medicine Lake demonstrate the link between magmatic processes and seismicity. For example, Dzurisin et al. (1991) find that subsidence and seismicity occur contemporaneously at Medicine Lake, and attribute it to a combination of crustal loading, Basin and Range extension, and cooling and crystallization of magma bodies. The clockwise rotation of the Oregon forearc causes extension at the block's southeast edge and drives the subsidence observed at Medicine Lake as well as the opening of the Oregon Basin and Range (Poland, 2006). Three clusters of earthquakes near Lassen Peak between 1936 and 1950, which included mainshocks up to M 5.5, are attributed to Basin and Range extension, though a magmatic trigger cannot be ruled out (Norris, 1997). Volcanism, magmatism, and plate motions associated with different tectonic provinces are all interrelated and help shape the faulting

patterns observed in the Pit River region. A recent study of strain indicators from seismicity in the Pit River region finds three interpretable clusters of similar earthquakes to the northwest, west, and southeast of the Pit River (Lahontan GeoSciences, 2012). All three clusters appear to have a component of dextral shear, but the western cluster has a component of compression while the northwest and southeast clusters show a combination of transtensional and pure dextral strike slip. This confirms that faulting in the Pit River region is complex, but that there are local zones of distinct stress.

The most prominent fault-related feature in the Pit River region is the Hat Creek graben to the southeast, which is bounded on the east by the Hat Creek Fault and on the west by the Rocky Ledge Fault and several others (Figure 2). Figure 2 shows how deformation morphology differs to the north and south of the Pit River; in particular, the distinct normal scarps of the Hat Creek graben do not clearly continue to the north of the river. Within the Hat Creek graben, bounding faults on both sides strike north to north-northwest. On the west-dipping Hat Creek Fault, total scarp height exceeds 500 meters in places (Muffler, 1994) and cuts flows as young as the 24±6 ka Hat Creek basalt (Turrin, 2007). The Hat Creek Fault stretches ~50 km along strike and is characterized by numerous left-stepping segments connected by relay ramps and monoclines (Muffler, 1994). On the west side of the Hat Creek graben, the east-dipping Rocky Ledge fault constitutes the largest member of the graben-bounding fault system. The Rocky Ledge Fault scarp stands 65-72 meters high, and the average slip rate on the Rocky Ledge Fault over the last ~200 ka is 0.4±0.2 mm/yr, an order of magnitude less than the late Quaternary slip rate on the Hat Creek Fault (Sawyer and Ramelli, 2012).

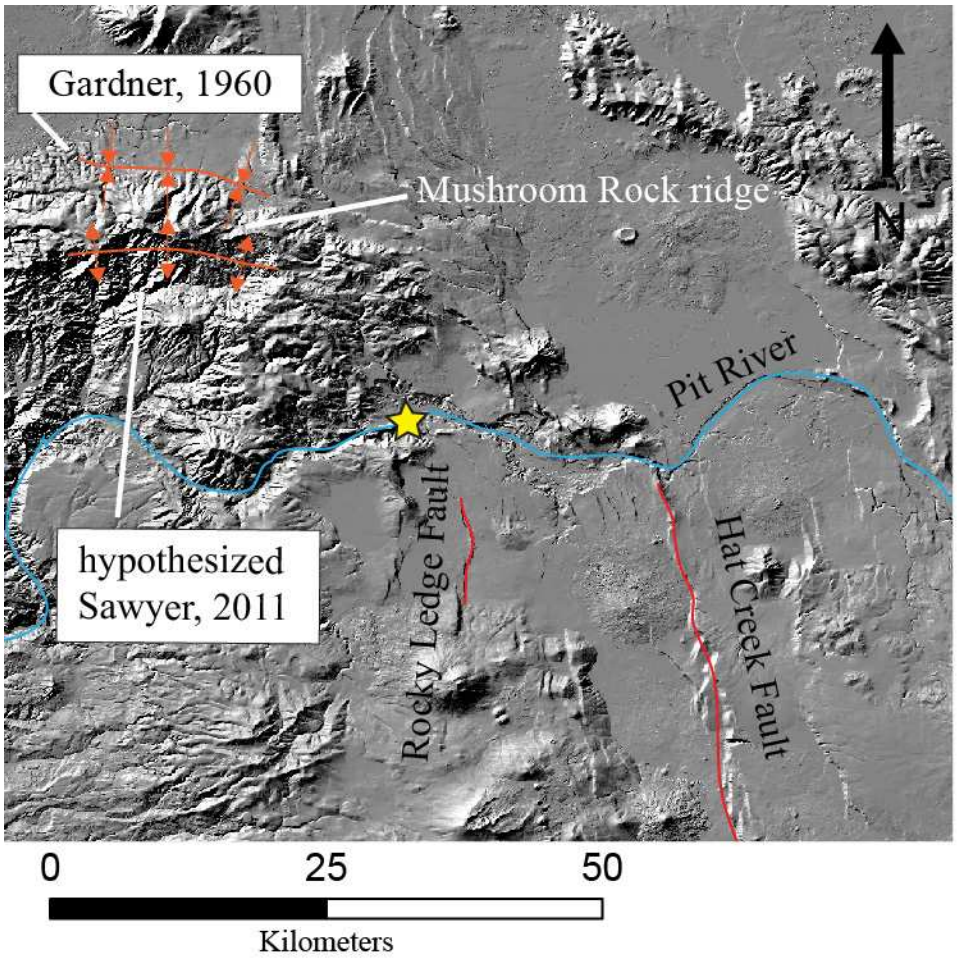

Figure 2. A regional hillshade map shows the location of the Pit 3 Dam and the Dicalite diatomite quarry, marked with a star. Shown in red are the two most significant bounding faults of the Hat Creek graben, the Hat Creek fault on the east and the Rocky Ledge fault on the west. Numerous north-south faults south of the Pit River become far less common north of the river, suggesting the transfer of strain to the west, perhaps via east-west compressional structures. To the northeast, the Modoc Plateau produces voluminous volcanism that is likely related to both Cascade backarc spreading and Basin and Range extension. High topography to the north of the Pit River and northwest of Pit 3 Dam exposes Klamath Mountains terrane rocks and is bounded to the north by a pair of potentially active folds near the Mushroom Rock ridge, suggesting north-south shortening consistent with the stress state in the Klamath Mountains block. Gardner (1960) mapped a syncline axis on the northern edge of the high topography, and Sawyer (2011) mapped a possible anticline axis bisecting the deep canyon just to the south of the Mushroom Rock ridge; both involve late Tertiary to Quaternary age volcanics.

Northwest of the Rocky Ledge Fault lies Lake Britton, where laterally extensive diatomite deposits are exposed, the thickest of which is excavated by the Dicalite

diatomite quarry (Figures 3 and 4). The diatomite overlies volcanic rocks as young as 1045.8±2.3 ka and is capped by the 973.6±12.3 ka Pole Creek Basalt, constraining the age to roughly 1 Ma (Muffler et al, 2012). The diatomite deposit formed when basalt flows dammed the Pit River at the eastern edge of figure 2, creating a large lake that covered much of the Burney-Pit River region. Diatomite deposits extend about 25 km to the east and are exposed in roadcuts and quarries and on the shoreline of Lake Britton.

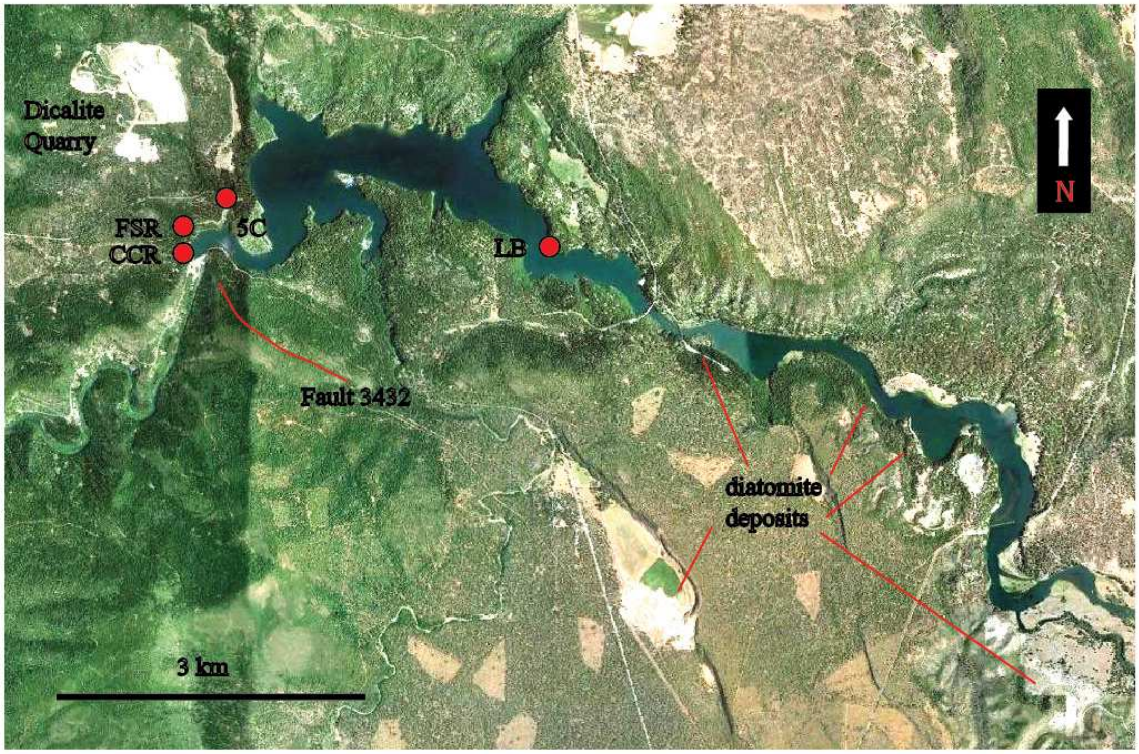

Figure 3. GoogleEarth imagery shows the Dicalite diatomite quarry and adjacent Lake Britton. Diatomite deposits are visible along the lake's shoreline, and in one location (LB) faults were sufficiently well exposed to allow measurement; fault plane orientation is consistent with faults in the Dicalite quarry and in the region. Three other external sites afforded good exposure of faults: Clark Creek Road (CCR) just north of the Pit 3 dam, Forest Service Road 37N05 (FSR), and the "Five Corners" intersection of Clark Creek Road and Forest Service Road 37N05 (5C).

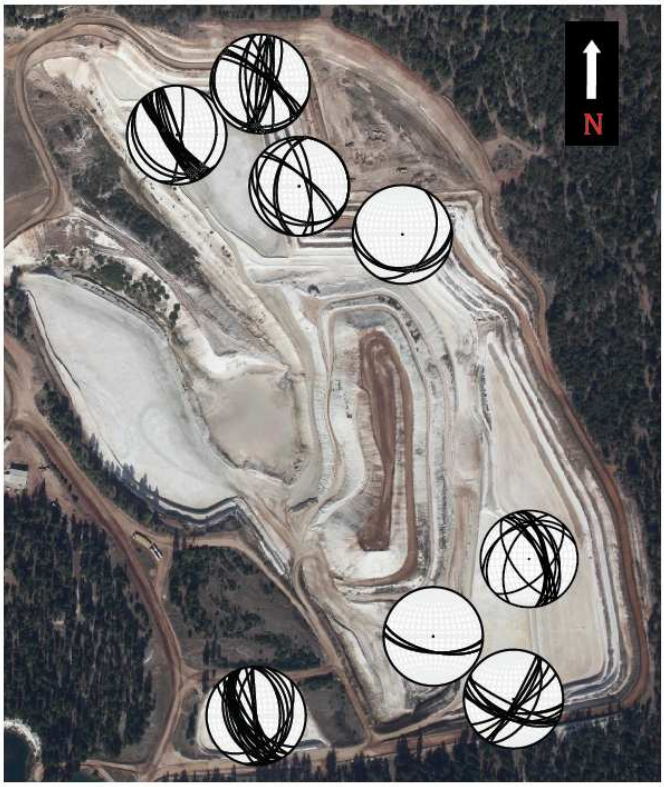

Figure 4. Aerial photography of the Dicalite diatomite quarry shows terracing that exposes faults. Many faults can be traced from the bench walls across the floor and into other benches. I measured faults along the entire outer perimeter, as well as on the floor where active mining was not occurring. Small stereonets show the distribution of faults in each location. The spiral-patterned form at the center of the quarry is a pile of overburden, which conceals any faults there. Photo credit: Dicalite Minerals Corp.

3. Motivation and goals for research

The motivation for research into the regional stress state near the Pit River is two-fold. First, we seek to understand faulting styles and crustal stresses in a transition zone between several distinct tectonic provinces. While much is understood about typical faulting styles in adjacent provinces, little work has been done at the intersection of these provinces and in particular how these boundaries may migrate or change through time. The Cascadia subduction zone and associated volcanic arc create compressive strain and volcanism (Murray and Lisowski, 2000); the Pacific-North American plate boundary produces right-lateral strike-slip motion concentrated on the San Andreas Fault and the Walker Lane-Eastern California Shear Zone (Dixon, 2000; Faulds, 2005); and the western Basin and Range is dominantly extensional (Hammond and Thatcher, 2004; Egger, 2011). All three styles of deformation – compression, extension, and horizontal

translation – have been observed to some extent in the Pit River region (Gardner, 1960; Muffler, 1994), which leads to several important questions. How are various deformation regimes distributed throughout the transition zone? Which type of deformation is currently dominant, and what has been the temporal progression of dominant stress states in the Pit River region? Which types of faults and offsets are expected to be active in future seismic events?

Second, faults in the region have the potential for surface rupture, which poses a potential hazard to people, buildings, and infrastructure in the region. By quantifying the regional stress state, we aim to help inform the hazard analysis of Fault 3432 (Figures 3 and 5), which projects northward toward the Pit 3 Dam near Burney, California. By determining the orientations of principal stress axes, we can infer the likely sense of slip on a fault with similar orientation to Fault 3432. Prior to this study, the sense of slip on Fault 3432 was not well documented. Several faults north of the dam have been proposed to be continuations of Fault 3432, so demonstrating a similar – or dissimilar – style informs the likelihood that Fault 3432 extends through the dam. Active faults south of the Pit River do not appear to continue across the river (Figure 2), suggesting a change in tectonic style or level of activity. Documenting the style of faults north of the river and how they compare with faults south of the river can help explain the apparent change at the river. The principle goal of the project was to use a statistically significant set of exposed faults from which to infer the regional stress state. A related goal was to determine if the stress state has evolved in the last ~1 Ma so that we could infer faults that are inconsistent in style with the current stress state to be inactive.

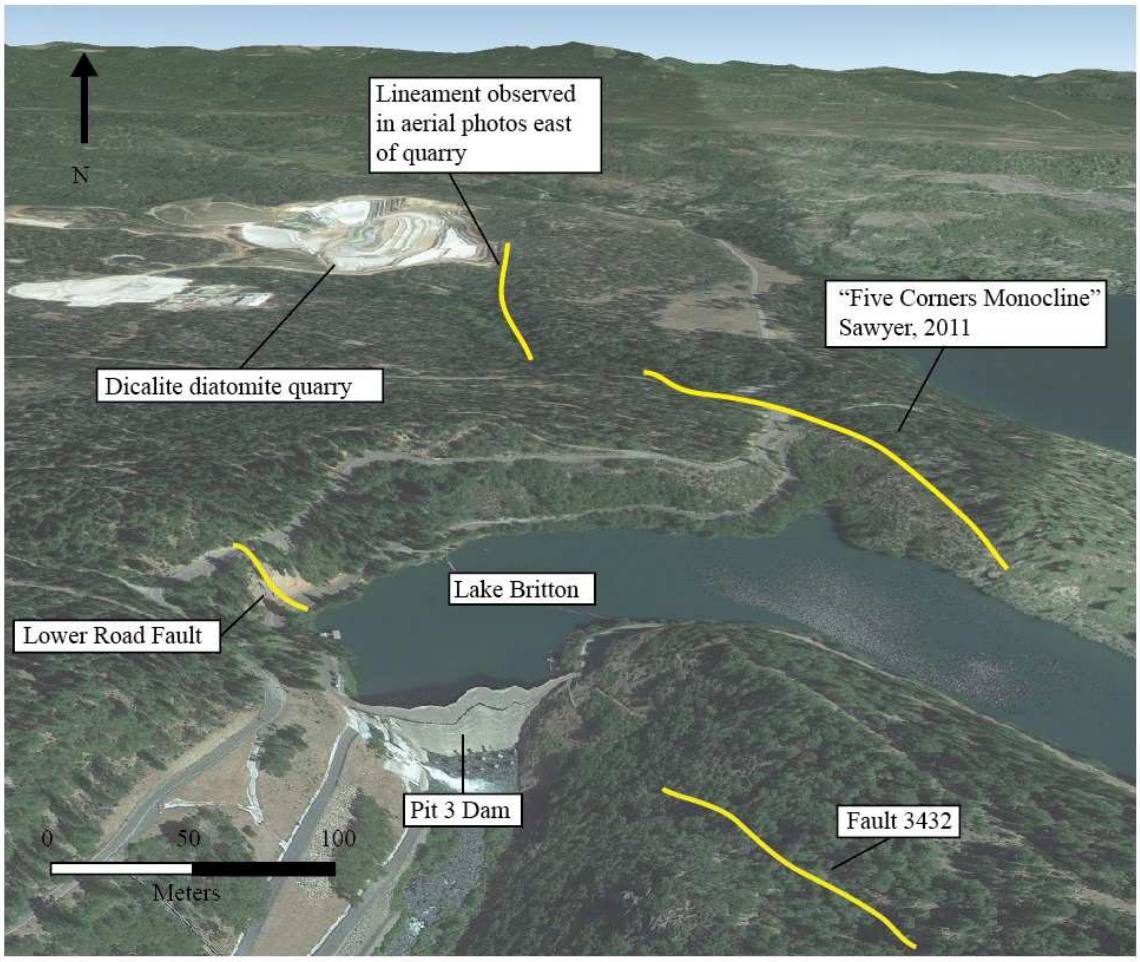

Figure 5. An oblique view of the western end of Lake Britton shows the proximity of the Pit 3 Dam to the Dicalite diatomite quarry where most of the fault measurements were taken. Also shown is Fault 3432, which projects toward the Pit 3 Dam, and the Lower Road Fault, which is visible in a roadcut north of the dam. In aerial imagery, a NNW-trending lineament appears to bound the quarry to the east. This is consistent with the gently east-dipping beds on the eastern margin of the quarry. We also show Sawyer's (2011) Five Corners monocline, which trends northwest and projects toward the diatomite quarry.

CHAPTER II

METHODS

1. Fault data collection

To determine the regional stress state, we measured the orientation of ~240 faults and 140 kinematic indicators on these fault surfaces. Kinematic indicators consist of slickenlines, or lineations, and mullions, or grooves that show the line of slip. Generally a unique direction, such as up or down a lineation, could not be determined, so additional information such as bedding separation was required to infer a unique slip direction. In order to infer the stress state for the greater Pit River region as opposed to a specific location within it, the set of faults measured and analyzed must average out local variations. We set out to find exposures of faults in as wide an area as possible (Figure 3), particularly in diatomite deposits because of their youth and excellent preservation of faults. By far the best exposures of faults and kinematic indicators exist in the Dicalite diatomite quarry, so we focused our efforts there (Figure 4). The Dicalite quarry north of Lake Britton and Pit 3 Dam is a ~100 meter-deep and ~1000 meter- by 500 meter- wide pit that provides excellent exposures of hundreds of small faults (Figure 6). Because the diatomite is underlain by volcanics as young as 1045.8±2.3 ka and capped by the 973.6±12.3 ka Pole Creek Basalt (Muffler et al, 2012), we approximate its age as ~1 Ma. Thus all faulting recorded in the diatomite is younger than ~1 Ma, which produces a fairly complete record of recent Quaternary fault activity. The scale of faulting varies in the quarry; several significant through-going faults can be traced for tens of meters across the quarry floor and through bench walls, and hundreds of smaller faults and fractures break up the areas in between.

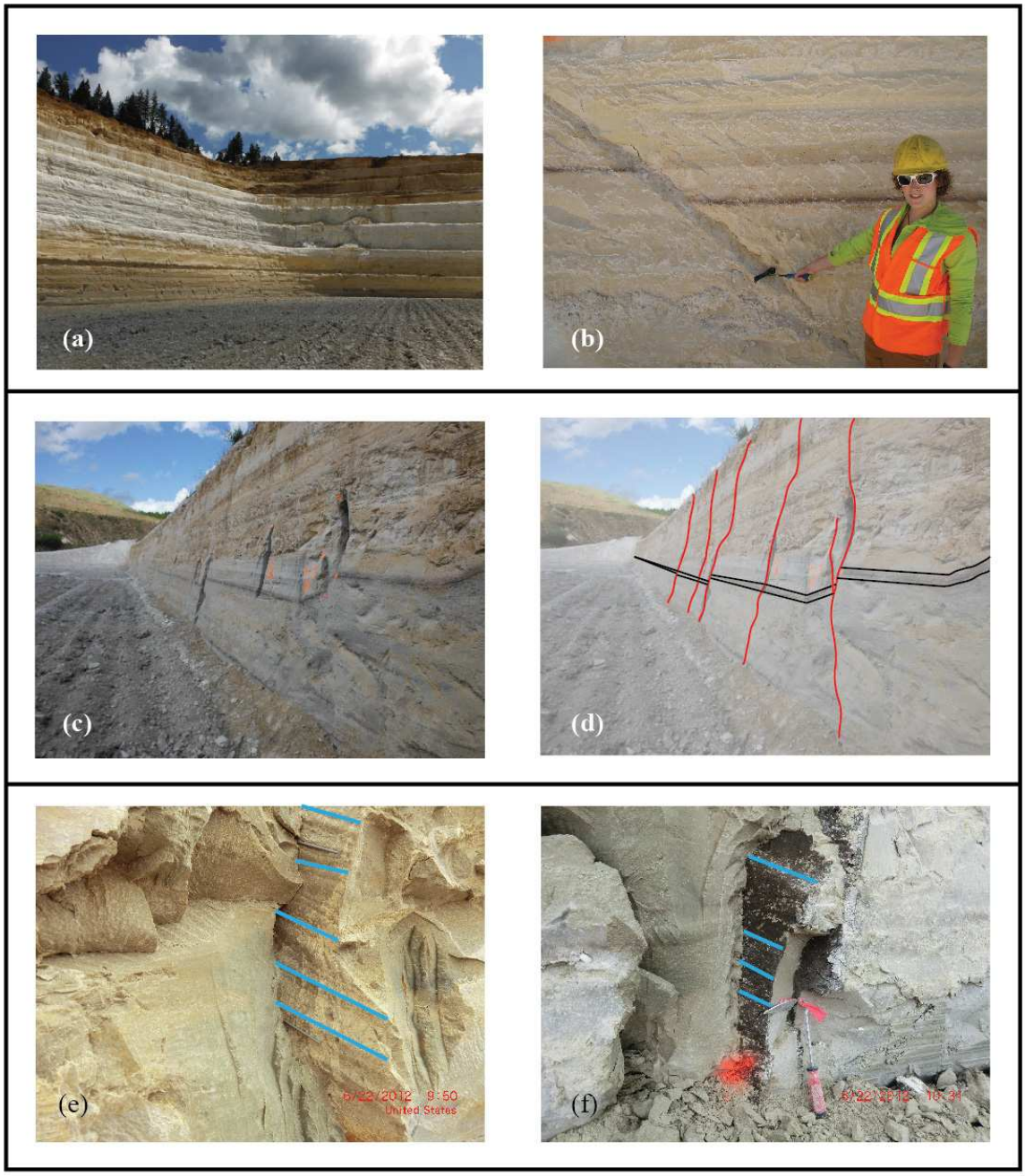

Figure 6. Relatively planar diatomite layers afford excellent fault exposures and preserve fault plane features remarkably well. The diatomite is soft, making it easy to dig out one side of each fault plane. Quarry walls were smooth until we dug out faults. Photo (a) shows vertical benches that provide exposures of offset bedding; photo credit Rocky Torgrimson. The vast majority of faults observed in the quarry showed normal separation (b) or no vertical separation. Photo (c) shows a number of faults offsetting a dark ash layer, highlighted in (d). The photos in (e) and (f) show well-defined fault mullions. Direction of slip on the fault surface as inferred from slickenlines and mullions is marked with blue lines; in both of these examples, kinematic indicators are subhorizontal on high-angle fault planes.

In the Dicalite quarry, diatomite is well indurated, and bedding is distinct and gently folded up to about 10°. Bedding varies in color, making it possible to trace specific beds along quarry walls, but there is virtually no parting of bedding planes or other evidence that it exerts a mechanical influence on faulting. By contrast, faults form discrete fractures along which the two sides can be separated, so it was easy to dig out one side of a fault plane to expose the fault surface and kinematic indicators.

I identified faults by bedding separation, spalling along the edge of the fractures, or discolored planes; I subsequently dug out one side to reveal the fault surface. While most faults broke out easily with a hand tool, faults with normal separation were difficult to dig out. On each fault surface I took two measurements, the orientation of the fault plane and the orientation of any observable kinematic indicators on the fault plane. Some faults were sinuous, in which the orientation of a fault plane varies over a short length scale; for these I took multiple measurements to appropriately document the variation and calculate an average. In many cases, centimeter- to meter-scale sinuosity of a fault plane is parallel to the kinematic indicators present on its surface. Though the majority of fault planes display well-preserved slickenlines (two-dimensional linear features; Figure 6f), mullions (three-dimensional raised grooves; Figure 5e), or both, some faults show poorly-developed kinematic indicators or none at all. In these cases, I only measured the fault plane. In total, I took 430 measurements on 243 faults, 231 within the Dicalite quarry and 12 faults from four locations outside of the quarry to confirm that the mine was representative of the region (Figure 7).

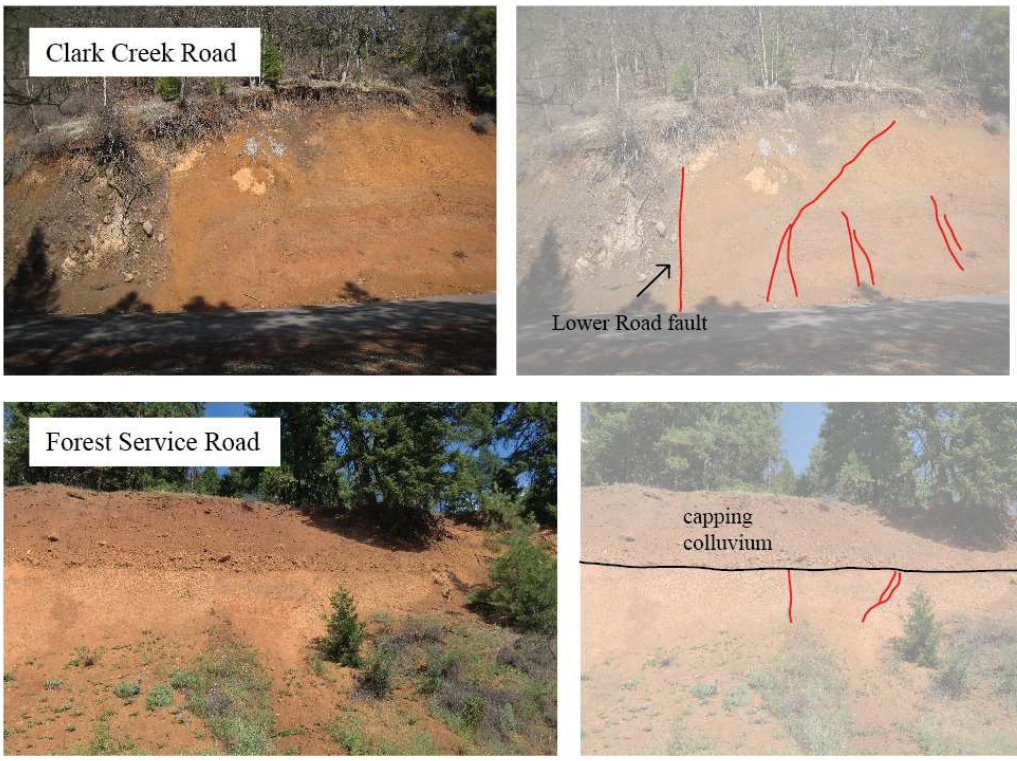

Figure 7. Of the four sites outside of the diatomite quarry, three are roadcuts and one is along the shoreline of Lake Britton. The Clark Creek Road roadcut exposes a large fault, the "Lower Road fault," which is part of the fault system that projects towards the Pit 3 dam. The roadcut on Forest Service Road 37N05 preserves two small faults that truncate into a capping gravel unit. The "Five Corners" intersection of Clark Creek Road and FSR 37N05 exposes faulted diatomite with many roots. Fault planes are likely acting as conduits for moisture, so kinematic indicators were poorly preserved on fault surfaces. The northern shore of Lake Britton exposed two faults whose orientations match two of the dominant geometries of faults in the mine. Lakeshore faults did not have any resolvable kinematic indicators.

The four sites outside of the diatomite mine are 1) in the northern roadcut along Clark Creek road adjacent to the Pit 3 Dam; 2) in the northern roadcut along Forest Service road 37N05 above the previous site; 3) in the eastern roadcut at the "Five Corners" intersection of Clark Creek road and Forest Service road 37N05; and 4) along the north shore of Lake Britton, east of the three previous sites and the Dicalite quarry (Figures 4 and 7). Within the quarry, I measured faults exposed along the perimeter walls on the north, east, and south sides (Figures 3 and 6). Wherever faults intersected, we attempted to determine if one fault offset another to establish cross-cutting relationships. At the center of the quarry, a large overburden pile obscures any measurable faults.

2. Fault stereonet analysis

We analyzed 430 fault plane and associated kinematic indicator measurements using stereonets to calculate the orientations of principal stress axes. As a first order analysis, we analyzed all high angle faults as a heterogeneous set on a single stereonet (Figure 8), excluding low angle faults, which were considerably less common and clearly inconsistent in likely stress orientation from high angle faults; these will be discussed separately below. We plotted all fault planes as poles to great circles and contoured the poles to find the orientation of the average fault plane. As will be discussed in detail in Chapter III, this average fault plane is consistent with the regional faulting pattern (Figure 2). We then plotted the average fault plane as a great circle along with all kinematic indicator measurements, which we refer to as slip vectors for our analysis; this enabled us to find the slip vector that best fits the average fault plane (Figure 8c). Using the average fault plane and slip vector, we can determine the orientations of the principal stress axes. The intermediate principal stress (sigma 2) is 90° from the average slip vector along the

average fault plane, and sigma 2 is the pole to the sigma 1-sigma 3 plane. The maximum principal stress (sigma 1) is ~30° from the average slip vector along the sigma 1-sigma 3 plane, and the least principal stress (sigma 2) is 90° from sigma 1 on the sigma 1-sigma 3 plane (Figure 8). Because this leads to two possibilities – sigma 1 can be 30° in either direction – we used observations of bedding separation to choose the correct one. A subvertical sigma 2 and approximately north-south sigma 1 suggests, on average, right lateral faulting essentially consistent with the Walker Lane zone, as will be discussed in Chapters III and IV.

To assess the spatial distribution of faults, we plotted fault planes and slip vectors from each individual location on separate stereonets (examples in Figure 9). Because similar orientations occurred at multiple sites (Figure 9) and discrete clusters appear in the contours of Figure 8, we subsequently plotted data from all sites on one stereonet in the form of poles to fault planes to determine if they fell into distinct sets based on fault plane orientation. Distinct clusters were apparent, so we started by grouping faults with obviously similar orientation, adding slip vectors to the plots, and calculating the principal stresses. We carried out several iterations of the grouping process, combining or splitting groups to find the most robust groupings. In some cases, we split groups that contained more than one set of slip vectors within a given fault plane orientation, with the goal of finding the best-defined groups of similarly oriented faults from all of the different regions. We settled on nine appropriate groupings and found the average fault plane and slip vector for each (Figures 10 and 11). Groups were principally selected by fault orientation, but in a few cases, distinct orientations of kinematic indicators were used to separate similarly oriented faults. Once groups were chosen, we found the

average fault plane and alpha-95 to check that the groups were actually distinct (Figure 10).

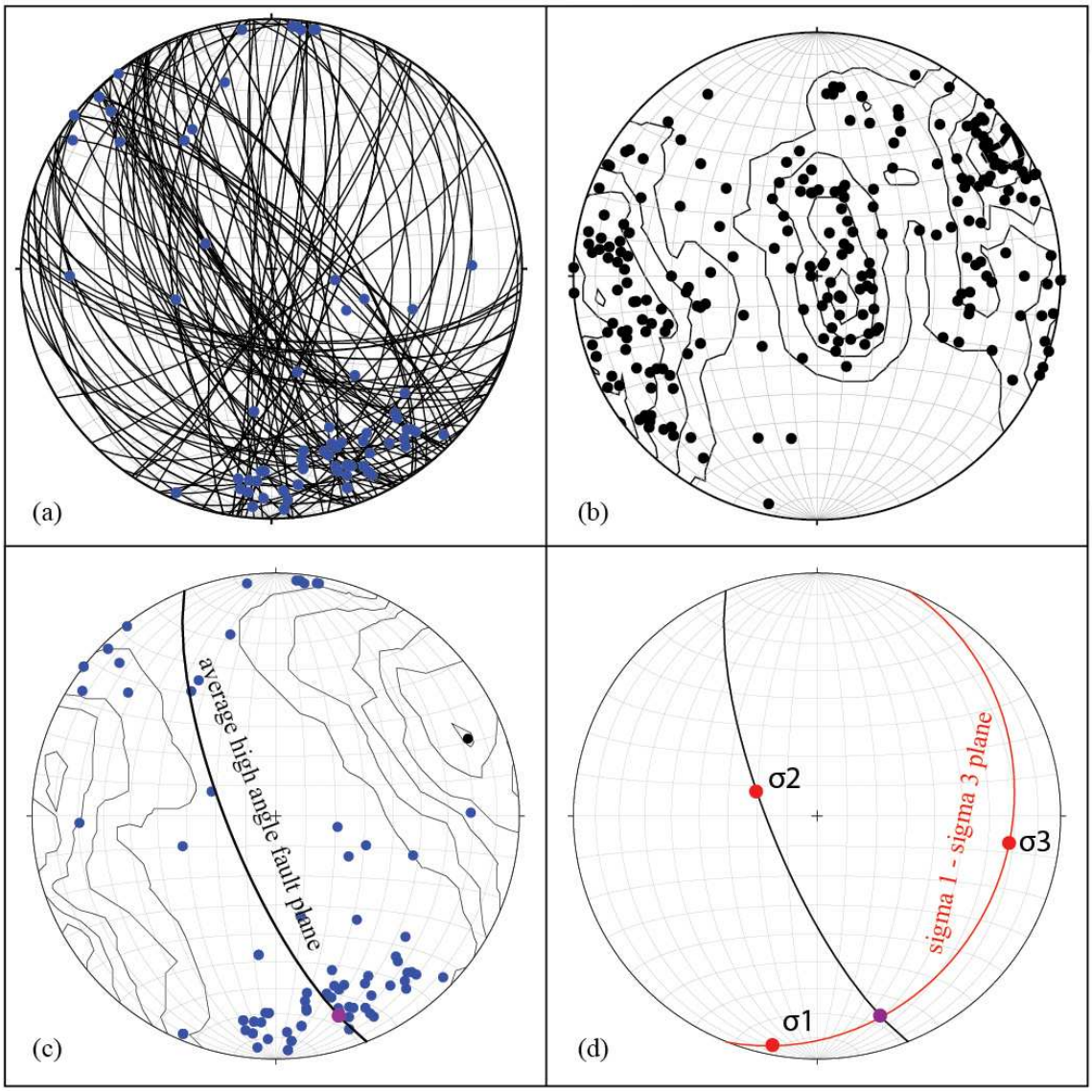

Figure 8. Stereonet (a) shows all measured fault planes (great circles) and their associated slip vectors (blue dots) where kinematic indicators were present and measurable (selected subgroups will be shown in subsequent figures). In stereonet (b), all fault planes are represented as poles (black dots) and contoured with Kamb contours. In (c), low angle fault planes are removed and the remaining poles to planes are contoured. The black great circle represents the overall average fault plane. Blue dots show slip vectors from all faults, and the purple dot reflects the average slip vector that falls on the average plane. Stereonet (d) shows the average fault plane and slip vector (as in (c)), and the principal stresses that would produce a fault of that orientation with slip in the direction of the average slip vector from (c). Note that most slip vectors in (c) fall on the sigma 1-sigma 3 plane, as would be expected.

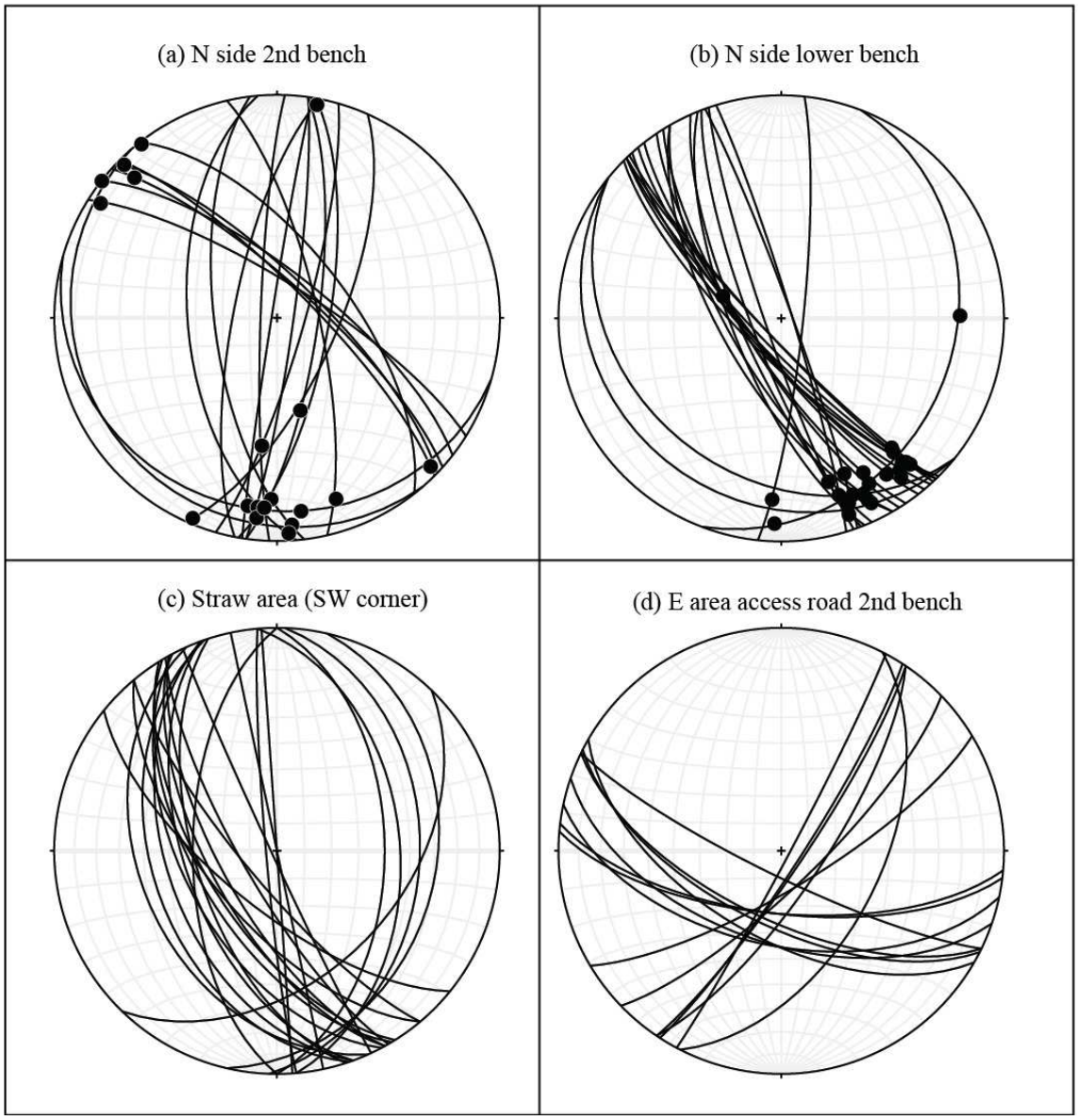

Figure 9. We originally grouped faults according to their locations within the diatomite quarry. These are four examples of the distribution of faults in a specific location. Some sites contain two groups of faults that appear to form a conjugate set.

For groupings determined by orientation, we found principal stress directions using two different methods. For each group, we used the average plane and average slip vector to find the principal stresses that would produce it, as described above. Six of the groups can be paired into what appear to be conjugate sets of faults; with this method, we

only used fault plane orientation, allowing us to make use of fault planes that lack kinematic indicators (Figure 12). In this method, sigma 2 is defined as the intersection of the average planes of the conjugate set, sigma 1 bisects the acute angle formed by the average planes, and sigma 3 is 90° from sigma 1 and sigma 2. Used together, these two methods provide a good system of comparison. For both of these methods, the underlying assumption is of Andersonian mechanics, that fault planes break at ~30° from the maximum principal stress or sigma 1 or bisect the acute angle of a conjugate set that is ~60° apart (eg. Twiss and Moores, 2007).

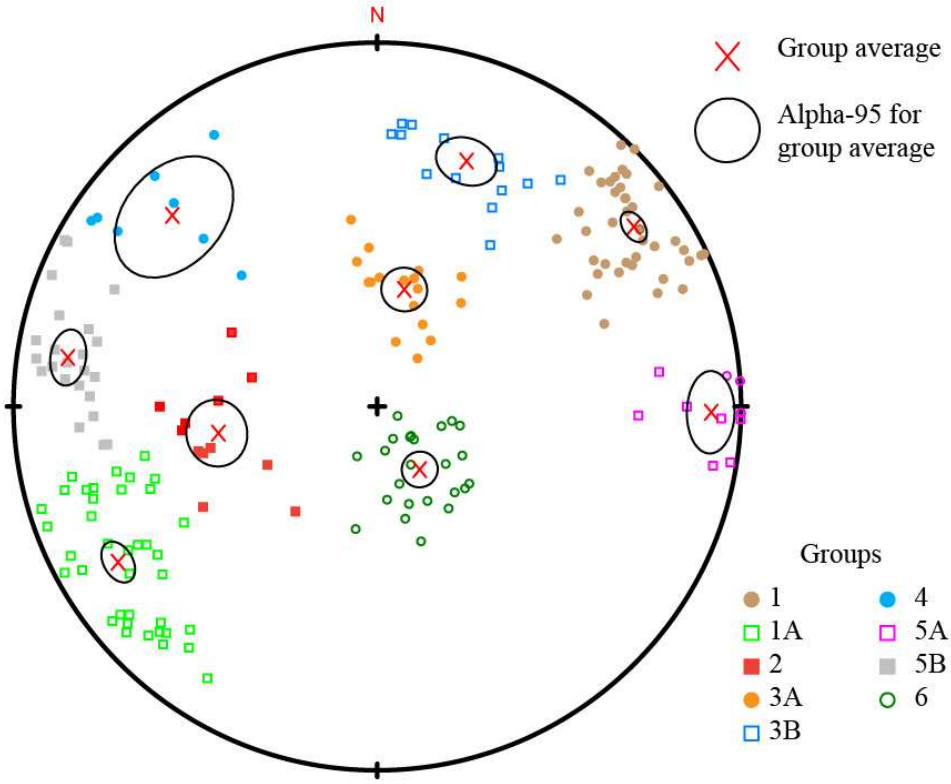

Figure 10. Fault plane and slip vector data are broken into groups of similar orientation and slip vectors. Here fault planes are shown as poles and separated into ten groups, marked with different colors and symbols. Because we carried out several iterations of groupings, some groups were created and subsequently split into two (here, numbers with A and B). For each group we calculate an average and alpha-95 using RockWare StereoStat; groups are distinct if group averages do not fall into any other alpha-95 regions. We leave out questionable data points and poles that do not clearly fit into a group, which make up about 15% of the faults measured; removed points can be seen by comparing to Figure 8b.

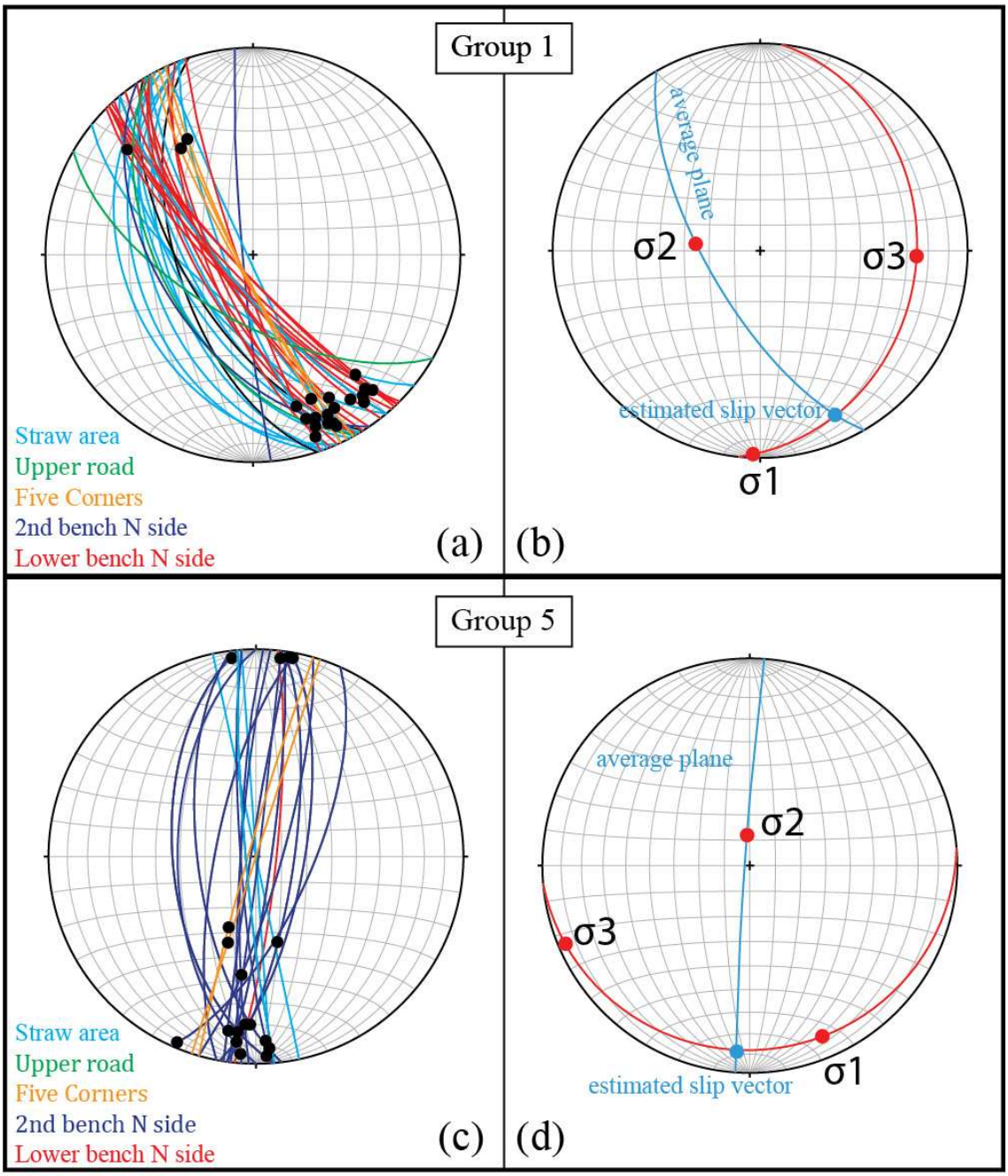

Figure 11. Two examples of grouping by orientation are shown with the solutions for stress state. From the set of faults in stereonets (a) and (c), we plot the average plane and average slip vector to find principal stresses in stereonets (b) and (d). Different colors in (a) and (c) reflect different locations where faults were measured; a variety of locations show similar fault orientations, supporting the idea that these faults are regionally representative. Note that the main clusters of slip vectors in (a) and (c) scatter along the sigma 1-sigma 3 planes in (b) and (d) respectively, supporting the inferred stress states.

3. Surveying in diatomite quarry and folding methods

To resolve folding within the diatomite quarry and to explore how low angle faults relate to bedding, we used high-precision surveying equipment, a Leica TCRP 1203 total station, to outline exposures of distinct marker beds throughout the quarry. Using monuments with known coordinates, we post-processed survey points by tying them to the monuments with known coordinates and translating them to their proper positions. Because the quarry walls are flat, we surveyed bedding around corners and curves in order to get a three-dimensional exposure from which we could extract a strike and a dip.

We calculated local bedding orientations by plotting elevation versus northing and elevation versus easting, and finding the slope of each. From these slopes, we calculated the distance to the north and to the east over which beds change one meter in elevation, which yields a right triangle. From here, the angles of strike and dip are easily found using simple trigonometry. To add to the bedding dataset, we also used original pre-mining drilling logs, provided by Dicalite, which included bedding orientations at each drill site. Some of the drilling log data were originally recorded as approximate or uncertain; we make note of these uncertain attitudes and use them sparingly in analysis. For an overall understanding of bedding attitude, we calculated a strike and dip from all survey points from a distinct layer exposed on three sides of the quarry, the Dicalite-named “Six Inch Ash” (Figure 18) We calculated fold axes by plotting all bedding data on a stereonet as poles to planes and fit a great circle to two elongate groups (Figure 19). The pole to this great circle is the orientation of the fold axis. We determined the position

of each fold axis on the map by using bedding dips as a guide: for example, we place an anticline axis between beds that dip away from each other in opposite directions.

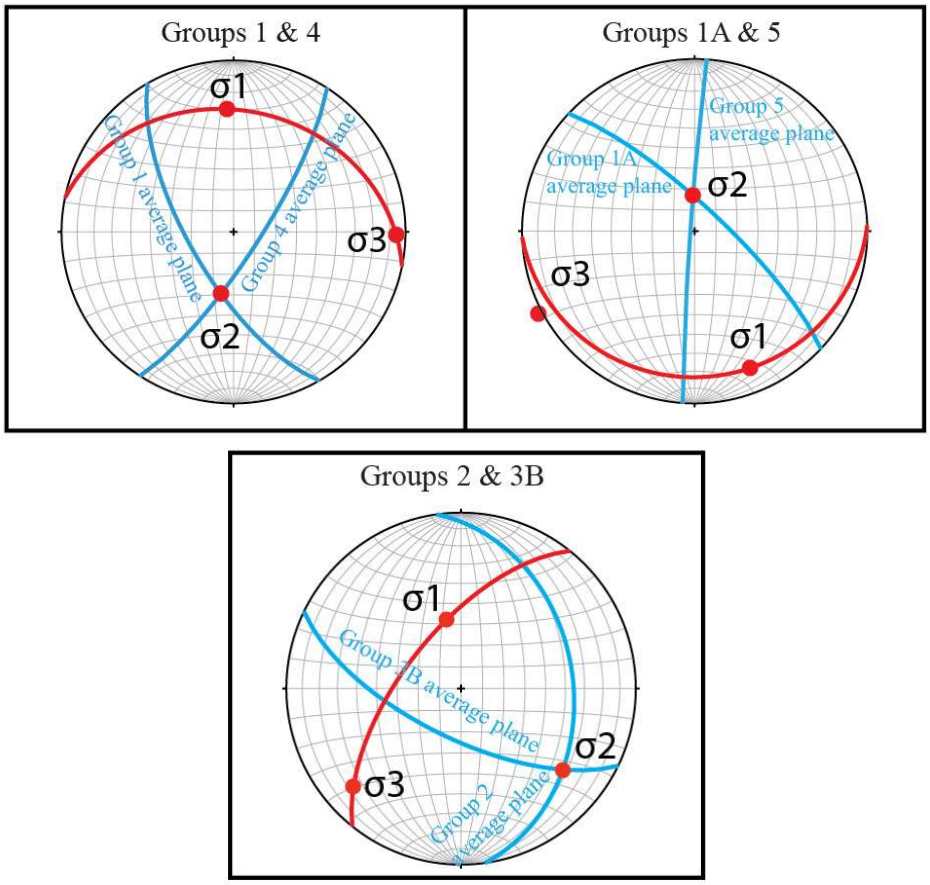

Figure 12. In these stereonets, we solve for principal stress directions using conjugate sets of faults, obviating the need for slip vectors. Here, the average planes of groups are highlighted in blue. According to Andersonian mechanics, the maximum principal stress bisects the acute angle between conjugate faults (eg. Twiss and Moores, 2007). The average planes intersect in sigma 2, and sigma 3 is 90 degrees from sigma 1 and sigma 2. These three stereonets reflect faults from six groups of faults separated by orientation. Note that the stress state solution for groups 1A and 5 agrees well with the solution for group 5 alone (see Figure 10).

CHAPTER III

RESULTS

1. Structural analysis

1.1. Whole dataset analysis

Plotting all high angle fault planes on a single stereonet and finding the principal stress directions yields a stress state that would produce right-lateral strike-slip faulting on a moderately dipping ~160°-striking fault plane, with sigma 1 trending 192° and plunging 2° (Figure 8). This orientation of fault plane is consistent with the dominant style of faulting observed in the region (Figure 2, especially south of the Pit River), and we see evidence of right-lateral strike-slip faulting in our slip vector dataset (eg. Figure 6e and 6f) and on the Lower Road Fault south of the diatomite mine near Lake Britton (Figure 7). The overall analysis of faults is consistent with a regional ~north-south sigma 1 associated with the Pacific-North American plate boundary and the local style of Walker Lane. However, many individual high angle faults and clustering in the pole plots (Figure 8) suggest that this average can be broken down into several discrete stress states.

1.2. Grouped analysis

In breaking fault plane datasets into nine groups based on orientation, we find that group averages and alpha-95s are distinct and distributed throughout the stereonet (Figure 10). Two of the high angle sets, groups 1 and 1A, contain a large portion of the dataset with almost 40 faults in each, and both are clustered tightly around their respective averages. These groups strike northeast and southwest and are essentially parallel but dip steeply in opposite directions (Figure 10). Several groups, 2 and 4, are more scattered but still have distinct averages and alpha-95s. Two other sets, groups 3A and 6, are made up

of very low angle faults and also form reasonably tight clusters (Figure 13). Both low angle groups have fairly consistent slip vectors, and the average planes of the two groups appear to form a conjugate set. In Figure 13, note that the slip vectors for groups 3A and 6 cluster along the sigma 1-sigma 3 plane in the conjugate set. Stress states derived from slip vectors and from the conjugate set are very consistent and show NNW shortening (Figure 14).

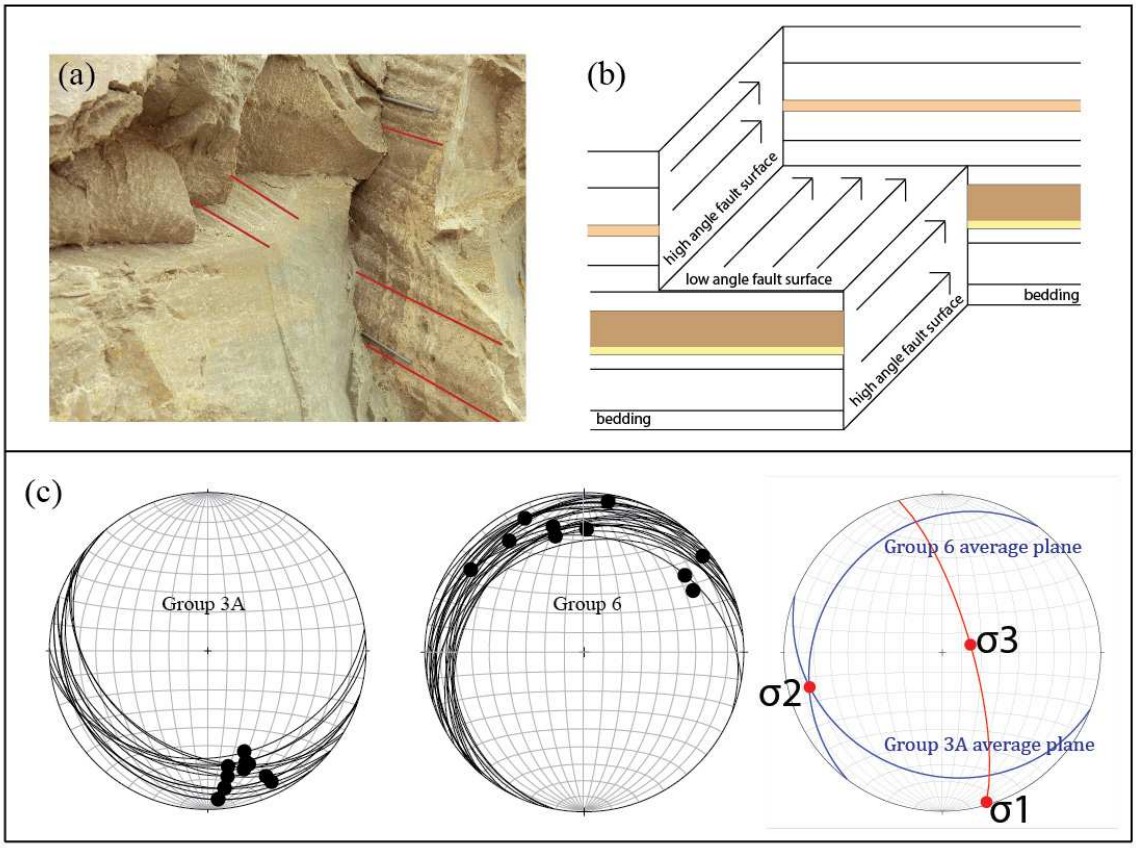

Figure 13. Because low angle faults seemed to be spatially associated with high angle faults (a), we initially hypothesized that low angle faults could be forming as accommodation structures for high angle faults, perhaps breaking along bedding planes, as illustrated in the diagram in (b). However, the orientations of fault planes and slip vectors are compellingly consistent (c) and form a conjugate set, suggesting that they result from a different stress state than the majority of observed faults. Note that in both groups, slip vectors cluster where the sigma 1-sigma 3 plane intersects fault planes, which adds strength to the interpretation that low angle faults reflect a distinct stress state. In addition, subsequent analysis of bedding showed that low angle faults did not parallel bedding.

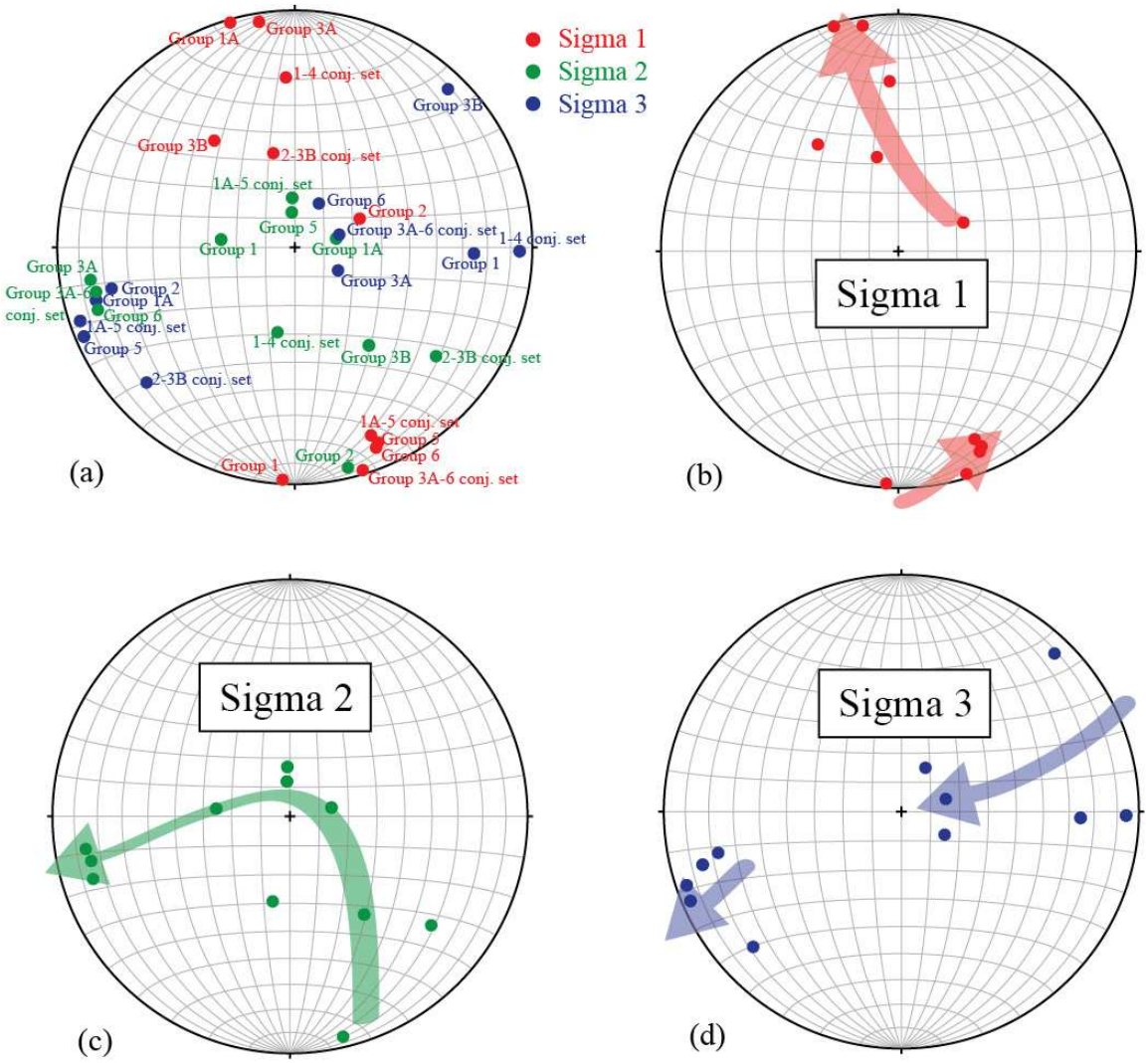

Figure 14. Summary plots of the principal stresses for each set of faults are shown in (a), with maximum principal stresses (sigma 1s) in red. Stress states cluster relatively well among the different groups, with the exception of the group 3A-6 conjugate set (see Figure 12). In (b), (c), and (d), we hypothesize the progression of each of the three different stress states with arrows showing the evolution of the stress field from oldest to most recent.

Principal stress axes for individual groups and conjugate sets are plotted in Figure 14. In general, there is good agreement between principal stresses determined from slip vectors and those found with conjugate sets. Principal stress directions from all groups and conjugate sets cluster along axes; the maximum principal stresses (sigma 1s) cluster

along a north-south axis and are mostly low angle, with the exception of group 2 (Figure 15). Intermediate and least principal stresses (sigma 2s and 3s) cluster along an east-west axis. The stress state for group 2 differs significantly from the majority of the groups' principal stresses with sigma 1 close to vertical, which indicates an extensional style of faulting consistent with separations seen across some of these faults. This is in contrast to the majority of principal stresses, which have a low-angle sigma 1, suggesting strike-slip or reverse motion (Figure 14).

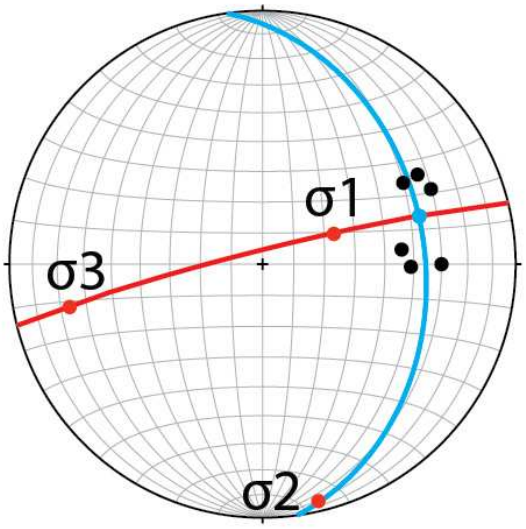

Figure 15. Group 2 shows a markedly different stress state than the other groups. Here we show how we derived the average slip vector and subsequently the stress state. The blue great circle on the right represents the average fault plane; black dots are all slip vectors from faults in group 2 (faults not pictured for clarity). We chose the average slip vector as the closest to the center of the cluster that lands on the average plane. From here, we find the principal stress directions based on Anderson's Theory of Faulting. Note that the stress state derived from group 2 alone differs from the stress state found from the conjugate pair of groups 2 and 3B (Figure 12).

Many of the faults that we observe to have strike-slip kinematic indicators dip at angles more typical of normal faults, and faults of the same orientation are observed to have both normal and strike-slip slickenlines. At several outcrops there appear to be conjugate normal faults from their orientations but have horizontal (strike-slip) slickenlines; this implies a shift in dominant stresses from normal to strike-slip. In Figure 14 we hypothesize the progression of regional stresses with normal faulting first, strike-slip second, and reverse faulting most recently.

Close examination of interactions between differently oriented faults does not give a consistent set of cross-cutting relationships (Table 1). In most cases, faults did not actually intersect; most clustered faults were subparallel or simply petered out before meeting another fault. And although many faults seem to interact in some way, we found no compelling evidence for one set of faults consistently cutting another set. When we observed two faults intersecting, the most common observation was that neither cut the other; they appear to pass directly through one another with no clear evidence for offset on either strand, indicating a conjugate set in many cases (Figure 16). Another interaction observed multiple times was a linear feature on the face of a high angle fault where a low angle fault intersects. We observe only one clear example of cross cutting relationships in the diatomite quarry (Figure 17), where a low angle fault offsets a high angle fault by several centimeters; also the high angle fault clearly offsets bedding subparallel to the low angle fault by several centimeters, so if the high angle fault moved after the low angle fault, it should be observable (Table 1 and Figure 17).

Table 1. Cross-cutting relationships from field notes. Here we document all locations in the quarry where faults intersect. Although many faults seem to interact in some way, there is little evidence for one set of faults consistently cutting another set. When two faults intersect, the most common observation was that neither cut the other; they appear to pass directly through one another with no evidence for offset on either strand. This suggests contemporaneous faulting, often as a conjugate set. Another interaction observed multiple times is a linear feature on the face of a high angle fault where a low angle fault intersects. While this is possibly suggestive of more recent low angle faulting, it could also reflect a remnant of low angle faulting preserved on a younger high angle fault. Either way, the linear feature is inconclusive. We observe only one clear example of cross cutting relations in the quarry, where a low angle fault offsets a high angle fault by several centimeters; the high angle fault offsets bedding by several centimeters.

Location	Fault names	Intersect?	Offset?	Comments
East area	62412M & 62412N	No	No	Project toward each other but do not intersect. Both high angle oblique; appears that north-striking fault dies out.
East area	62412P, unnamed	Yes	No	Floor of east area. Faults pass through each other but do not offset at all. Unnamed is E-W with many en echelon steps; both high angle with no kinematic indicators.
N side 2nd bench	62712K	Yes	No	Conjugate-looking set but w/ sub-horizontal slicks. No offset. Appear to have only minor slip below intersection.
N side 2nd bench	62812I & 62812J	Yes	No	Conjugate set? Intersect but no offset. Bedding offset normal on I; I difficult to dig outo. J has strike-slip indicators.
N side 2nd bench	62812K & 62812L	Yes	Possibly	Linear feature on high angle K where low angle L intersects, but minimal to no offset. Small offset of K by L?
N side 2nd bench	62812M & 62812N	Yes	No	Low angle N does not project straight across high angle M, possibly resulting from low angle N forming after existence of M.
N side 2nd bench	62812O & 62812P	Yes	No	Low angle O bends and forks at high angle P, as if P was already there when O formed. Beds not offset by P.
N side 2nd bench	62812Q & 62812R	Yes	No	Low angle Q deflected/folded at high angle, as if high angle R was already there. See photo in figure 17.
N side 2nd bench	62812S & 62812T	No	No	Low angle T stops at high angle S. Both faults offset bedding only minimally.
N side 2nd bench	62812Z & 62812A	Yes	No	Linear feature on high angle fault A where low angle Z intersects; no offset. Neither has significant bedding offset.
N side 2nd bench	62812C & 62812D	Yes	No	Linear feature on C where low angle D intersects, but no separation/offset.
N side 2nd bench	62812GG, HH	Yes	No	Low angle conjugate. No offset.
NE corner	62912X, Y, Z	Yes	No	Higher angle Y separates low angle X by 4 cm. Y and low angle Z intersect; linear feature on Y where Z intersects, but no offset. Conjugate?
NE corner	62912I & 62912J	Yes	Yes	Low angle I offsets high angle fault J that has normal separation. Only clear example of cross-cutting.

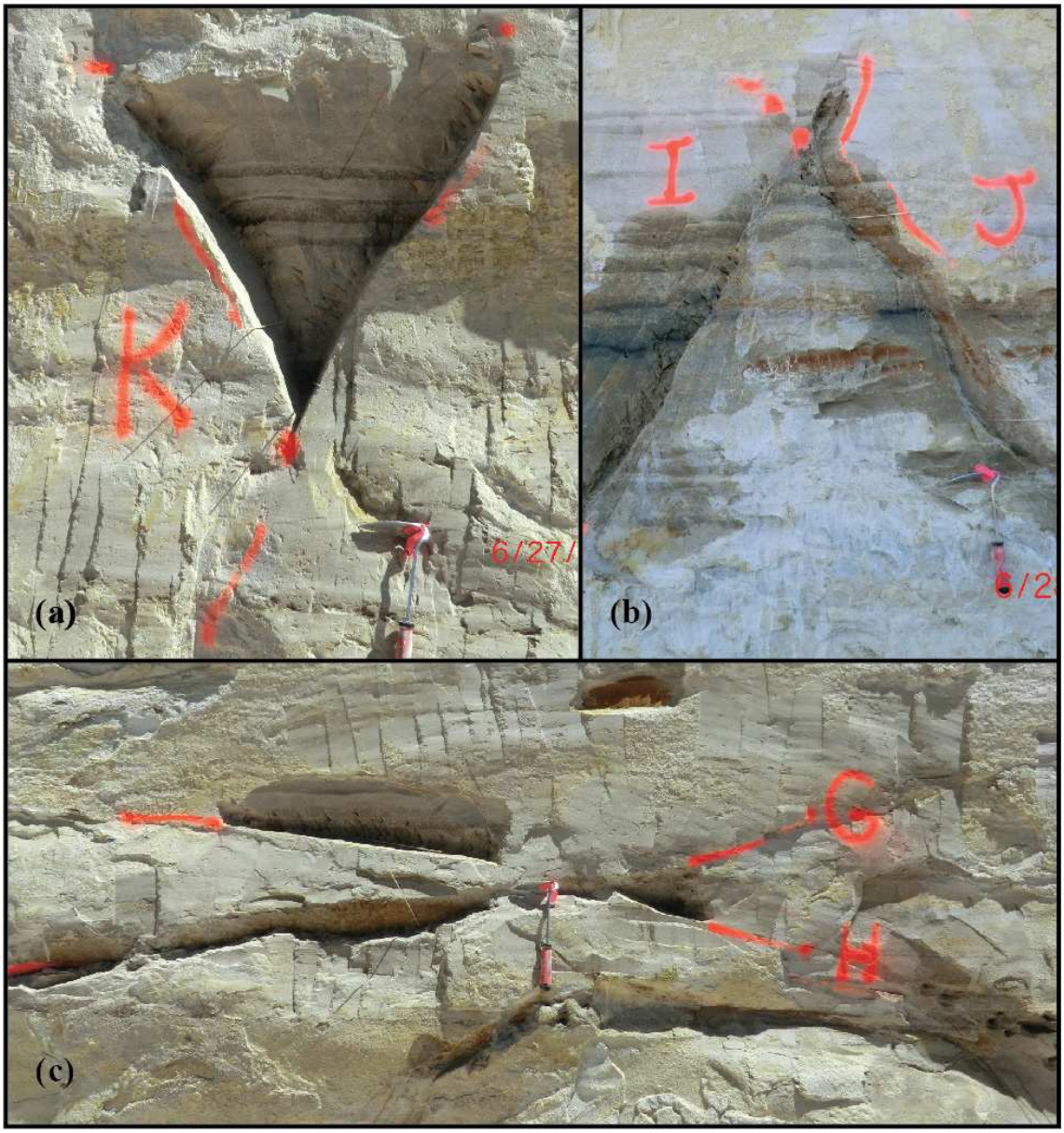

Figure 16. Photos of conjugate faults in the diatomite quarry show several things. In (a) and (b), faults appear to be conjugate normal faults that formed during an extensional regime. In both cases, faults have been reactivated as strike-slip or very low angle oblique; both faults in (a) have subhorizontal kinematic indicators, and the fault on the right in (b) has subhorizontal kinematic indicators. We could not obtain a slip vector for the left fault in (b), as it did not dig out easily. The two faults in (c) represent a low angle conjugate set. This particular wall faced west, so north is to the left in the photo and south is to the right; this is significant because the orientation of faults implies north-south shortening, which we see further evidence of in fault sets and folds.

2. Surveying and folding results

Bedding data calculated from survey points agree relatively well with bedding data extracted from many of the Dicalite drilling logs (Figure 18 and 19) and show evidence for at least seven subtle folds in two distinct orientations (Figure 20). Two synclines correspond with the paleochannel filled by diatomite (Figure 21), which has led mine operators to speculate that folding is due to draping or compaction into paleotopography. However, the consistency of those folds with others that do not follow paleotopography suggests that this relationship is coincidence, and that folding is instead due to tectonics. In addition, units thicken to the NNW (Figure 18), not into the troughs of synclines as would be expected if folds reflected the draping of diatomite onto paleotopography.

The overall bedding attitude calculated from the "Six Inch Ash" has a strike of 38° and a dip of 5°, meaning that overall the bedding dips slightly to the southeast; this is confirmed by correlating composite drill logs from the quarry, which show beds thinning and dipping to the southeast. Fold axes determined by stereonet analysis of poles to bedding data occur in two sets, one set, F1, trending 137° and plunging 4°, and a second

---

Figure 17 (next page). Examination of cross cutting relationships does not reveal any consistent relationship; however, we emphasize several important observations. 1) Low angle faults seem to be associated with high angle faults: rarely do they occur without the presence of adjacent higher angle faults. 2) Faults interact in some way, and many tend to intersect and not obviously continue on the other side (c). In particular, the presence of high angle faults affects the geometry of low angle faults (a), possibly suggesting that the high angle fault was there when the low angle fault formed. 3) Low angle faults are not parallel to bedding. (b) is the only clear example of cross cutting that we observed in the quarry. In this case, the lower angle fault offsets the higher angle fault, which in turn has offset bedding. More common are two intersecting faults that appear to pass directly through one another with no evidence of any kind that one existed first (c). Bedding is offset on the floor of the quarry by a fault in (d).

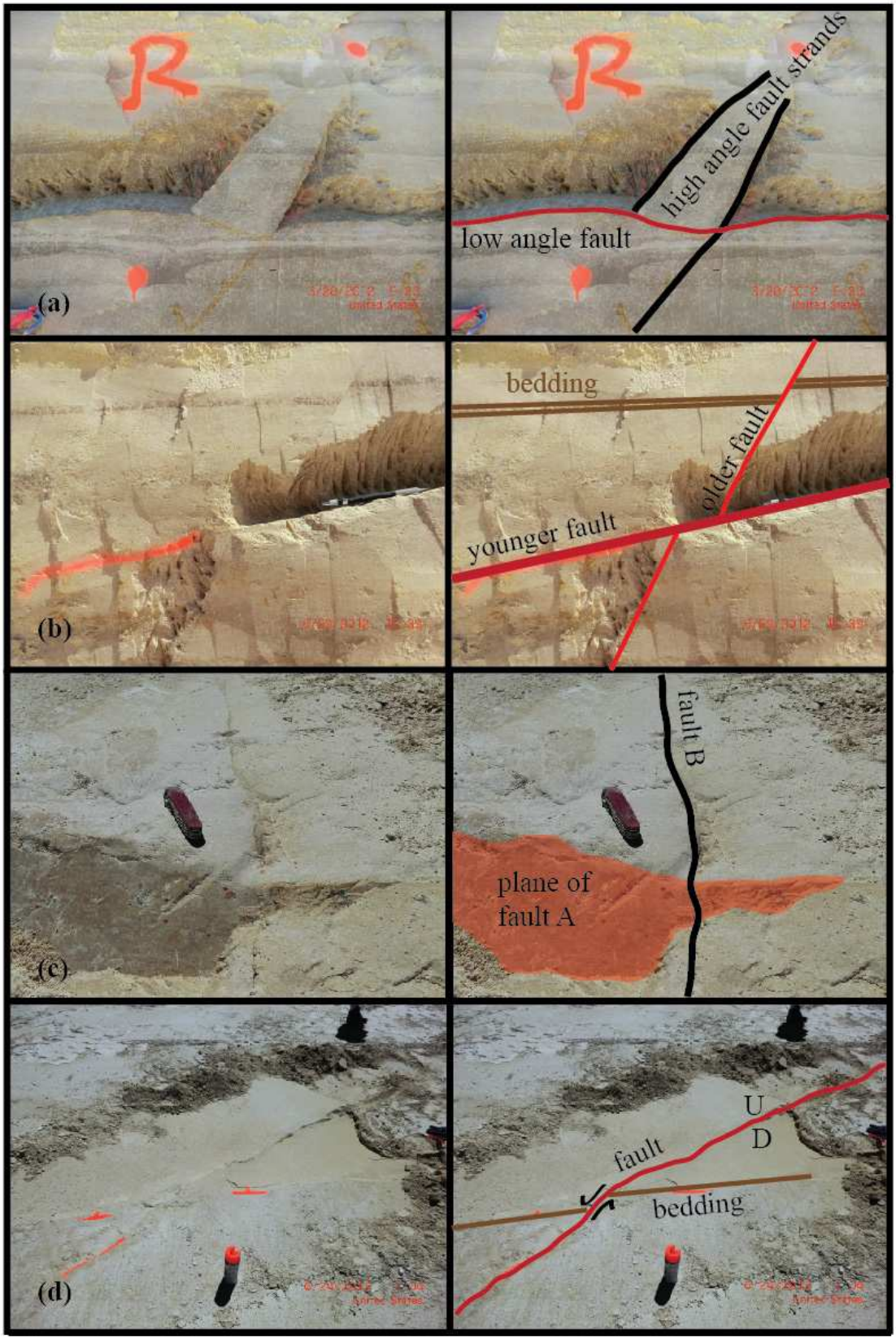
(a)
high angle fault strands
low angle fault
(b)
bedding
older fault
younger fault
(c)
fault B
plane of
fault A
(d)
U
D
fault
bedding

set, F2, trending 216° and plunging 2° (Figure 20). When fold axes are untilted by returning the average bedding to flat, F1 becomes essentially flat, and F2 does not change significantly. Since F1 folds become flat and the average dip across the entire mine is consistent with the folding of F2, we infer that F1 occurred first and F2 occurred more recently.

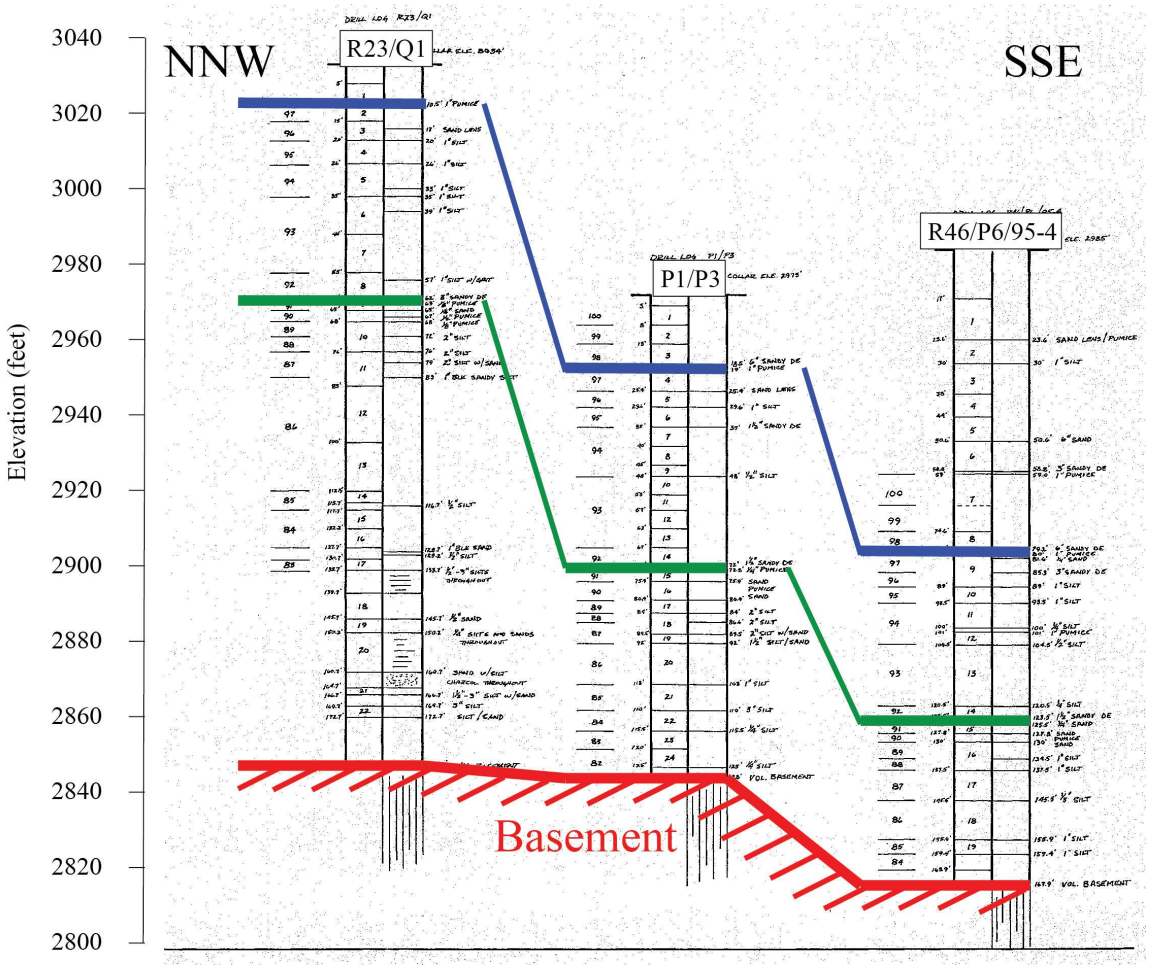

Figure 18. Correlation of original composite drill logs from the Dicalite mine shows beds both dipping and thinning to the SSE. Each composite log is the combination of two or three adjacent drill sites with similar stratigraphy. Blue and green lines represent distinct beds that can be traced throughout the mine, and red represents basement rock. The tops of each section were removed by erosion to various depths and are not indicative of bedding thickness. Composite log R46/P6/95-4 is at a low in the bedrock where a tributary joined the paleochannel and shows the thinnest stratigraphy. The averaged locations of the three composite drill logs are shown in Figures 19 and 21.

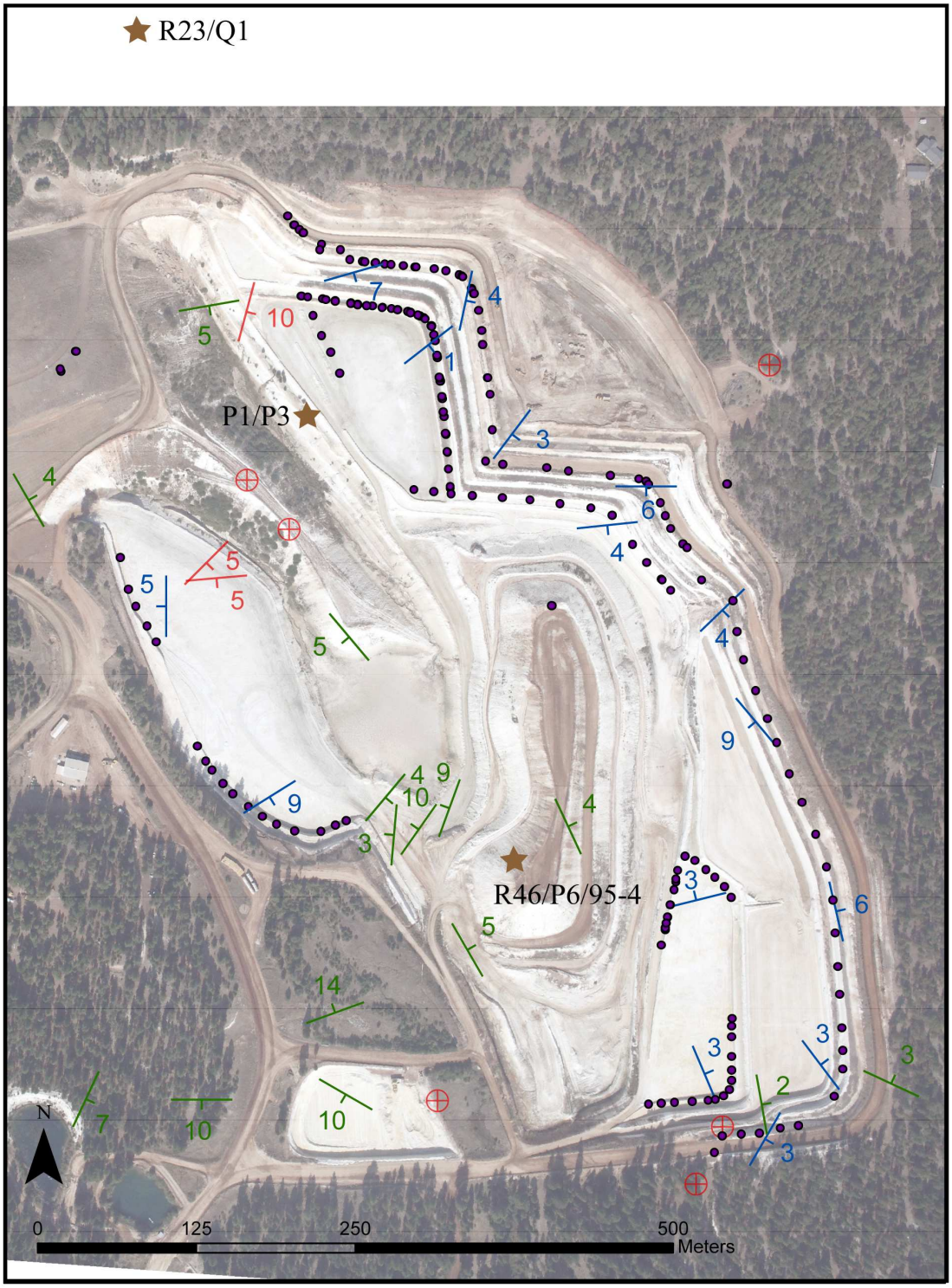

Figure 19. Survey data from the quarry are shown as purple dots. We followed distinct units where exposed, focusing on corners and curves in order to calculate bedding attitudes. Blue bedding symbols represent measurements calculated from the survey data; green bedding symbols indicate robust measurements from drill logs; red bedding symbols represent questionable or uncertain measurements from drill logs. Stars show average location of composite drill logs from Figure 18.

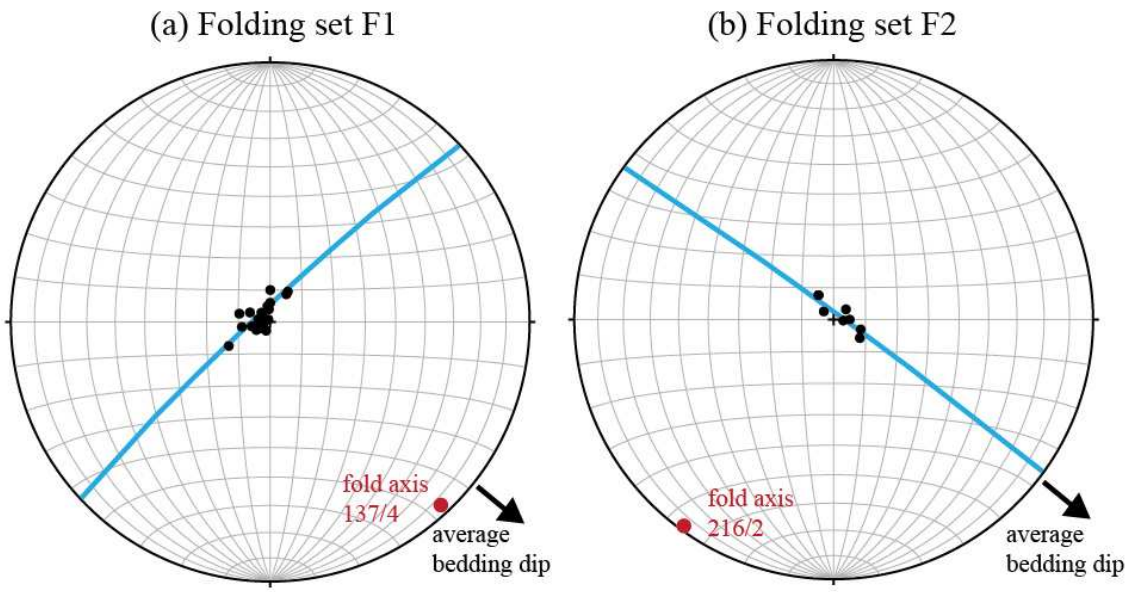

Figure 20. Plot of poles to bedding planes from the quarry, which we acquired through surveying and from drilling records. We find that they fall neatly into two sets: F1, with poles clustered along a NE-trending plane and F2, with poles clustered along a NW-trending plane. The poles to these planes constitute the fold axes and trend 137° and 216°. Bedding orientations consistent with F1 are more common and more widely distributed than F2, which are found only in the west central part of the quarry. Using the surveyed Six Inch Ash across the entire mine, we found the average orientation of bedding, which strikes 38° and dips 5°. This is consistent with a limb of F2. If we unfold F1 based on F2, the axis of F1 becomes flat.

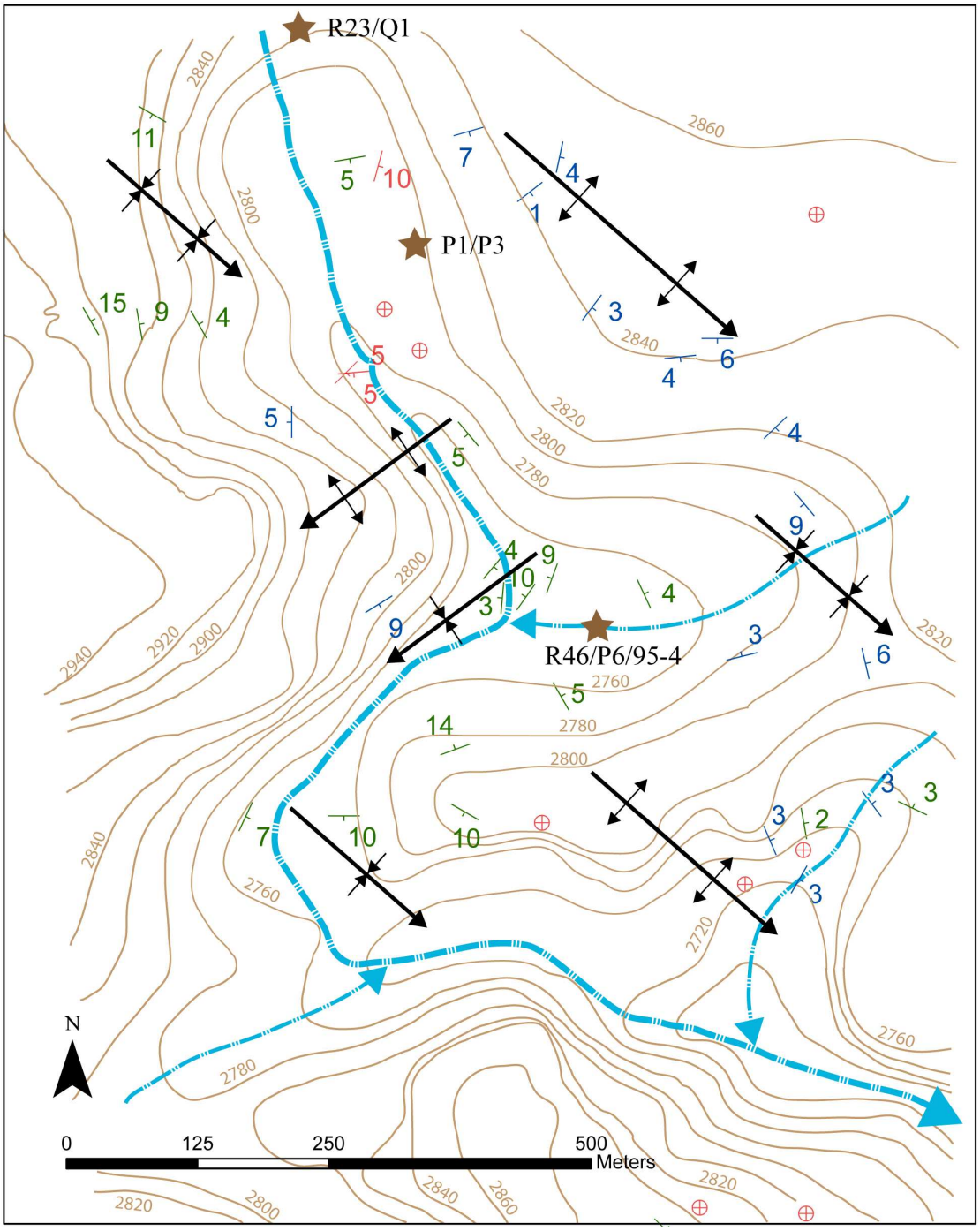

Figure 21. Basement contours from original Dicalite drilling logs are shown in brown. Labeled units are in feet; contour interval is 20 feet. Stars show the average locations of composite drill logs from Figure 18. Bedding attitudes are overlain with same color scheme as previous figure (survey measurements in blue; robust drill logs measurements in green; uncertain drill log measurements in red). Pre-diatomite drainage pattern is shown in light blue. We find two generations of folds (calculated as shown in Figure 20), one with an axis that trends ~137° and one trending ~216°. Bedding orientations from the majority of the quarry fit into the first set, while bedding matching the second set is confined to the central section (the westernmost mined section).

CHAPTER IV

DISCUSSION: STRESS STATE EVOLUTION

In this chapter we discuss the likely evolution of the stress state immediately north of the Pit River from normal faulting to strike slip to reverse. Because we found few compelling cross-cutting relationships, we rely mainly on evidence of reactivation of faults, the overall pattern seen in the range of the stress states we document, and the tentative evidence suggesting that the low angle faults represent the most recent stress state preserved in the diatomite.

Group 2, with a vertical sigma 1 and east-west sigma 3, reflects an extensional stress state that we argue is no longer active. Abundant regional evidence exists in support of a long period of extension, with much of it clustering on the south side of the study area near the Hat Creek and Rocky Ledge Faults. South of the Pit River, the period of extensional faulting extends at least back to the time of the diatomite deposition. Diatomite clearly was deposited into the Hat Creek Graben and likely across the Hat Creek Fault zone. The lack of obvious extensional faulting in the area covered by diatomite is likely due in part to the burial of pre-existing faults. In and adjacent to the diatomite quarry, we find a few high angle faults with dip-slip indicators on their fault planes. While most high angle faults have dips suggestive of normal faults, almost all have subhorizontal slip indicators, which is what we would expect to see if the stress state had been predominantly extensional and subsequently changed to a strike-slip dominated regime. While the orientations of fault planes in group 2 scatter somewhat (Figure 10), their slip vectors cluster well and allow a confident selection of an average slip vector for analysis (Figure 15). We interpret group 2 as evidence for a purely normal stress state

that existed in the last million years – hence the inclusion of group 2 faults in the 1 Ma diatomite – but is no longer active. When group 2 is combined with group 3B and analyzed as a conjugate set, the result differs from the individual analyses of the groups. While it would be easy to dismiss the groups as not conjugate, I argue that some of the scattered group 2 faults formed contemporaneously with group 3B faults or were reactivated where appropriately oriented into a conjugate set. Analyzed alone, group 3B gives a stress state that is still more extensional than all other groups, so associating groups 2 and 3B makes sense. Assuming that the stress state changes through time in a tectonically active transition zone, groups 2 and 3B fit cleanly into the progression (Figure 14). Given the progression shown in Figure 14, two possibilities exist, normal to strike slip to reverse, or reverse to strike slip to normal. Abundant field evidence of normal faults reactivated as strike slip faults favors the former sequence, as does folding and tentative cross cutting evidence for late compression discussed below.

In the analysis of all measured faults together, we find a right-lateral strike-slip stress state, which is consistent with the majority of measured faults and many regional structures, including the Lower Road Fault adjacent to the diatomite mine to the south. Stress states for the dominant groups 1 and 1A support the whole set analysis, and we infer that a dominant signal for high angle faults with strike-slip to oblique motion reflects a significant and regional stress state that is more recent than the extensional stress state that produced faults in group 2, but is not currently the active stress state north of the Pit River. Given the ample evidence for strike slip faulting, it is likely that a strike slip regime dominated for most of the one million years since the diatomite was deposited. On either end of the stress state progression, we can resolve different stress

states: we see the end of normal faulting early in the diatomite's history, and we see the beginnings of a reverse overprint on top of strike slip faulting.

Two sets of tightly clustered low angle faults, groups 3A and 6, are evidence of what we infer to be the most recent stress state in the Pit River region, which suggests NNW compression and shortening. Fault planes and kinematic indicators for low angle groups 3A and 6 cluster tightly (Figure 13). In particular, slip vectors for each set cluster at the intersections between the sigma 1-sigma 3 plane and the groups' respective fault planes. This would be very unlikely to occur if the faults were random accommodation structures or due to landsliding or compaction within the mine. Additionally, the average bedding dip in the mine – to the southeast – does not correlate with either low angle group, which means that low angle faults were not simply exploiting bedding planes. In detail, individual low angle faults dip in opposite directions to local bedding. Regional evidence of large-scale folding in the Mushroom Rock region to the north of the Pit River (Figure 2; Gardner, 1960; Sawyer, 2011) also hints at north-south shortening. The ridge along Mushroom Rock, which runs generally east-west, is thought to be the axis of a growing anticline (Sawyer, 2011); this is consistent with a syncline axis mapped parallel to Mushroom Rock ridge to the north where the slope meets the plateau (Gardner, 1960).

While most cross-cutting relationships observed in the mine are inconclusive, the single clear example of cross-cutting involves a low angle fault offsetting a high angle fault by several centimeters; the high angle fault offsets bedding by several centimeters (Figure 17). This supports the progression of high angle oblique normal to strike-slip faulting to low angle compressional faulting. The majority of cross-cutting relationships are between high angle faults and suggest contemporaneous faulting, sometimes as

conjugate sets of faults (Figure 16). In a region at the intersection of such diverse tectonic provinces, it is reasonable to expect that, with the continuous evolution of stress states and overwhelming dominance of the intermediate strike slip regime, one might expect a lack of clear cross-cutting relationships.

The two generations of folding in the diatomite quarry also reflect two different stress regimes. F1 occurred first, possibly as monoclines associated with buried normal faults in an extensional stress state, and F2 occurred subsequently, folding F1 and diatomite beds gently to the southeast. F1 folding is parallel to other regional normal faults and monoclines and clearly predates F2 folding. This progression of stress states supports the progression found by analyzing faults and shows recent compressional stresses forming characteristic faults and folds. Also, bedding determined by surveying is not consistent with the idea that low angle faults exploit bedding as planes of weakness.

CHAPTER V

CONCLUSION

Through the analysis of faults and folds near the Pit River, we determine that the regional stress state has evolved over the past million years. Four main observations allow us to infer the progression of stress states from extensional to translational to compressional: (1) evidence of normal faults reactivated as strike-slip faults (Figure 16), (2) the overall pattern seen in the range of stress states (figure 14), (3) the sequence of folding determined from surveying in the mine (figure 21), and (4) one clear example of a low angle fault cutting a high angle fault (figure 17).

Evidence for an oldest extensional regime consists of a set of northwest-striking high angle faults with dip-slip kinematic indicators; this is consistent with structures like the Hat Creek graben in the greater area. The extensional regime transitioned to a strike-slip dominant regime that is consistent with Walker Lane, and many high angle faults that originally had normal slip were reactivated as strike-slip or oblique faults. During this time the Lower Road Fault was active; however, it does not cut late gravels that overlie it, implying that the stress state has continued to change. Two sets of low angle faults, one clear example of a cross-cutting relationship, and a generation of compressional folding are evidence of a recent shift to a more compressional stress regime. While it is certain that the regional stress state has evolved through time, it is also likely that the stress state varies spatially on the scale of a few to tens of kilometers based on crustal structure and lithology, making it possible for normal faulting to occur on the Hat Creek Fault contemporaneously with oblique faulting on the Rocky Ledge Fault and compressional faulting and folding near the Dicalite diatomite quarry and Mushroom Rock to the north.

The pattern of faulting observed in the Pit River region forms a continuum with distinct sets of faults: to the southeast, NNW-striking normal faults are dominant; south of the Pit River near Fault 3432, north-south-striking right-lateral strike-slip faulting dominates; north of the Pit River near the diatomite mine, we observe north-south compression beginning to overprint previous stress states. Fault 3432 likely formed in a normal stress state and slipped as a strike-slip to oblique fault for most of its history. Its current activity likely terminates at the Pit River because its orientation is such that it cannot slip in the current stress state north of the river. As regional tectonic stresses evolve in the future, faults will continue to reactivate in different ways and accommodate strain through a variety of orientations of faults and folds.

Within our dataset of faults less than 1 Ma in the vicinity of the Dicalite diatomite quarry and the Pit 3 Dam, the majority occur as strike-slip to slightly oblique, with a small percentage of normal and reverse faults that form distinct sets. This signifies that for most of the last million years, the regional stress state has been largely transcurrent, producing strike-slip faults, with short but distinct periods of extension and compression.

APPENDIX A

FAULT MEASUREMENT FIELD DATA

Clark Creek Road 2-Apr-12

Fault plane	Location	Strike	Dip	Dip direction	Trend	Plunge	Comments/ quality of kin. indicator
4a	Furthest east in series of faults along roadcut.	N58W	89	W	N74W	57N	Lower surface
4b		N75W	87	NE	N78W	48N	Upper - plunge not great
3a	Several meters west of fault 4.	N65W	79	W	N74W	29N	Upper - good
3b		N59W	75	W	N69W	26N	Lower - not great
3c		N73W	83	E	N72W	34N	Left fracture
2a	East of fault 1 by several meters (right when facing outcrop).	N48W	76	W			Lower
2b		N42W	79	W	N74W	58N	Upper - poor
1a	Adjacent to fault 5, several meters to east (right when facing outcrop).	N80W	80	W	N86W	34N	Top - decent
1b		N38W	71	W	S76W	62N	Lower - okay
5a	Adjacent to main fault (fault 6), several meters to the east (right when facing outcrop).	N56W	63	W	S36E	31S	Upper - okay
5a		N47W	88	W			Lower - not visible
5a1		N44W	66	W			Middle, slightly to the left
5b		N03W	47	W	S48W	34S	Good quality
5c		N72W	89	W	S82E	76S	Poor quality
5d		N51W	75	W	S48E	24S	Upper - okay
6a	Main fault. Furthest west of series of faults (left when facing outcrop).	N45W	73	E	N50W	8N	Middle, very good quality
6b		N50W	69	E	N46W	13N	Lower - good
6c		N47W	74	E	N46W	6N	Top - good

Five Corners 20-Jun-12

Fault	Location	Strike	Dip	Trend	Plunge	Photo no.	Kinematic indicator	Comments
62012A1	N of Five Corners	155	84	330	10		Mullions	High
62012A1.5	N of Five Corners	155	84	156	12		Mullions	High-mid
62012A2	N of Five Corners	151	83	331	8	237-240	Mullions	Low-mid
62012A3	N of Five Corners	153	84	154	16	241-243	Large scale mullions	Parallel plane on fault
62012B1	N of Five Corners - east of A	198	90	198	54		Faint slicks	Mid-high

62012B2	N of Five Corners - east of A	196	87	200	60	244-245	3 good mullions	Photo 246: overview of outcrop

Upper FS Road 1-Jul-12

Fault	Location	Strike	Dip	Trend	Plunge	Photo no.	Kinematic indicator	Comments
A1	Large roadcut on slight left curve. Above & slightly east of lower road fault.	328	87	332	36	774-787	Shape of fault	Part of network of several larger faults and some smaller faults/fractures covering the roadcut. Same lithology as lower road (tuffaceous sandstone), capped by gravel/colluvium. These faults do not cut the capping gravel/colluvium.
A2	Same as above	150	54			774-788		
A3	Same as above	120	64	252	56	774-789	Slicks? Or roots?	
B1	Same as above	321	83	324	38	774-790	Mullions - decent	
B2	Same as above	308	84	328	22	774-791	Mullions - decent	

Lake Britton 2-Jul-12

Fault	Location	Strike	Dip	Photo no.	Comments	
1	Northern shore of central Lake Britton, west-facing outcrop	326	66	870	Right (south)	Significant faults in sandstones interbedded with silty diatomite. Parallel, distinct structures with no kinematic indicators due to roots and hydrologic exploitation of fault planes.
2		325	66		Middle	
3		326	66		Left (north)	

Fault	Location	Distance from west end (ft)	Strike	Dip	Trend	Plunge	Photo no.	Kinematic indicator	Comments
62212A1	"East wall" - north side lower bench	13.9	150	68	152	11	249-252	Mullion- only one. Not obvious	Photo 253-254: stratigraphy on wall 2m east of A
62212B1		22.8	343	86	165	18	255-258	Mullion?	Base of fault
62212C1		31.9	340	86	168	26	259-264	Average	Base
62212C1.5		31.9	340	86	165	24		Great mullions	Base
62212C2		31.9	161	84	166	25			20 cm above C1
62212D1	"East wall" - north side lower bench	89.5	6	82	183	20	277-281	Slicks & small mullions	D1 & D2 are in left strand of two branch fault. R strand has ~25 cm of apparent offset in dark brown layer, but fault itself not well developed. On L strand, fault breaks out cleanly with nice slicks & small mullions, but little to no apparent offset.
62212D2		89.5							
62212E/1		108	150	71	157	14	265-266	Excellent mullions & decent slicks	Base, ~20 cm from ground. Dark brown, damp gouge layer ~1 cm wide. At base (~75 cm from ground surface), stepover ~8 cm. Lower strand dies out and slip focused on upper strand above ~80 cm.
62212E/2		108	156	75	160	13	267-269	Lg mullion- large enough to rest Brunton on	Near stepover. 20 cm above E1.
62212E/3		108	158	72	163	8	270-273	Mullions- small, subtle	Mullions & slicks less obvious on this surface b/c gouge layer broke during excavation, thus I am looking at center of gouge layer.
62212E/4		108	159	79	163	8	274-277	Slicks in far gouge edge	
62212F1		114	138	77	142	15	284-287		Base of fault. Some sort of splay occurring, with L strand less prominent but with more apparent offset, and R strand more prominent but with less apparent offset.
62212F2	"East wall" - north side lower bench	114	135	76	140	16	284-287	Slicks	~20 cm above F1

62212F3		114	142	78	148	17	288-289	Slicks & small mullions	
62212G1		121	136	80	143	14	291-293	Mullions	Top, near dark brown layer
62212G2		121	136	78	140	17	294-295		Large face below G1
62212H1		147	136	83	144	25	296-299		Top
62212H2		147	137	83	142	23	300-301	Slicks	Mid-low. Slicks abundant and convincing; seem to be steeper than mullions, as well as better quality.
62212I1		153.6	146	76	157	23	303-305	Mullions	Top
62212I2		153.6	140	78	149	12	306-307	Slicks	Mid-low
62212J1		157.6	181	90			308-311		Top. No kinematic indicators visible.
62312K1		92.7	129	30	154	18	315-318		Left side
62312K2		96.9	129	19	154	13	315-318		Left side, right of K1
62412M1	"East area" - lg flat bench above trench		252	32	58	12	332-333	Striations-bedding?	Significant fault breaking out along floor of east area- intersects other faults including lg (~25 cm separation) fault on wall of east area. Fault plane of M breaks out easily; appears to be a dominant feature. Can follow for tens of meters.
62412M2			235	28	51	5	395-398	Slicks? Mullions? Bedding?	East of M1. M is sinuous/wavy. Apparent indicators perhaps bedding or mineral deposits? Sinuosity and large scale gentle mullions suggest subvertical motion.
62412M3							399-400		M3 is on wall and connects to M1 & M2 on floor. Cm-scale separation visible on wall. Tracing M3 upward, it projects to but does not intersect/reach N set of faults (that dip SE).
62412N1			44	56	206	19	334-338	Decent mullions	Part of a set of parallel faults traceable from wall (east) to floor. Normal separation of 2 cm along fault in wall.
62412O1	"East area" - lg flat bench above trench		352	65			339-340	No obvious slicks or mullions	Fault system running parallel to wall in east area. Appears to take many steps, mostly to the left.

62412P1			146	61	244	56	349-352	Good subvertical mullions	Significant fault breaks out nicely on floor and projects/can be followed back to wall fault with significant separation (~25 cm). Same fault as in photo from Oct with Katie. *P intersects smaller fault system characterized by SE dip, SE-side down separation, and many right steps. Smaller steps w/in strands are both right & left. Face of P does not appear to be broken where other fault system intersects. (see photos 341-348)
62612Q1	"East wall" - north side lower bench	179	180	74	3	6	451-453	Good slicks	
62612R1		197.1	7	70	186	16	454-456	Mullions- not great	This fault splits into many subparallel strands and extends up the wall. Mullions are inconsistent, measurement given is best estimate.
62612S1		216.3	11	85			457-458		
62612S2		216.3	45	68	231	53	459-460	Mullions	S1 & S2 have different orientations but appear to be part of the same fault system. No appreciable kinematic indicatiors on S1; S2 has well defined mullions that curve with fault plane. S2 may be a rotating block instead of a distinct fault.
62612T1		220.5	204	90	200	33	461-462	Slicks	Front face of multi-strand fault system; subsequently removed to access T2.
62612T2		220.5	22	86			463-464		Fault T has significant separation (~ 20 cm) on wall, but lacks a coherent fault plane. There are at least 5 different planes, but no one breaks out dominantly.
62612T3		220.5	202	90	196	44	465-467	Slicks & mullions	T3 main fault plane?
62612T4		220.5	28	86	23	30	468	Mullions	T4 antithetic/mullions inconsistent?
62612U1		232.6	2	90	4	12	469-471	Mullions?	Nice plane, but very little in the way of kinematic indicators. Maybe mullions? Not entirely convinced.
62612V1	"East wall" - north side lower bench	238.5	4	71	164	42	472-474	Mullions- okay	Faults V are above folded brown layer, part of fold system. Mullions not great; slicks are better.
62612V2		238.5	5	75	158	56	475-477	Slicks	

62612W1		256.3	75	40			478-481		"Faults" W are questionable - they appear to be simply fracture planes where walls are breaking off - but I keep seeing planes of similar orientation breaking out, and "mullions" appear to be oriented similarly. Reasonably sure they are not faults, however.
62612W2		258.6	68	34			478-481		
62612X1		265.8	125	84	141	14	482-483	Slicks?	Again, not entirely convinced this is a fault as opposed to a fracture breaking off. Questionable.
62612Y1		273.6	82	43	210	40	484-486	Mullions?	Same issue as W, but beautiful mullions of some type.
62612Z1		302.9	208	80	210	67	487-489	Slicks & mullions	Nice fault with normal separation of 7 cm on wall along fault. Breaks out decently. Slicks & mullions appear steep, and are only okay in quality.
62612A1		279	290	60	110	12	490-493	Slicks	Debatable. Nice plane, decent slicks.
62612B1		282	120	53			494-496		NOT a fault, but I'm curious about orienation of these failure planes.
62612C1		333.3	320	78	320	51	497-500	Mullions	Separation in brown layer above ~1 cm
62612D1	"East wall" - north side lower bench	340.9	10	79			501-504		Separation of 8 cm total, ~2 cm over D1. Appears normal, west block down, but could also be reverse, with east on top? More of a fold than faults. No appreciable slicks or mullions.
62612E/1		374.6	15	71	178	44	505-507	Slicks & mullions	Good fault w/ separation. Slicks & mullions agree.
62712F1		10.9	8	75	348	56	508-510	Slicks	Nice fault. Relatively no separation.
62712G1		77.8	16	80	0	42	511-512	Slicks + small mullions - decent to good	Total 5 cm separation over 3-4 different strands. G1 roughly middle strand. West side down (apparent).
62712H1		92.0, 93.2	189	88	186	16	514	Mullions-nice	Fault system H is a system of diagonal faults, subparallel, that offest dark bed ~25 cm with west side down separation. Overall photos 513, 516.
62712H2	"East wall" - north side 2nd bench	92.0, 93.3	8	84	181	16	515	Mullions-decent	
62712H3		92.0, 93.4	347	75	158	16	517	Slicks & mullions-	

								decent	
62712H4		92.0, 93.5	10	71	182	11	518	Slicks-ok/decent	
62712I1		110.5, 113.6	139	11	176	10	519-523	Great mullions!	Can follow only a little (~20cm) in each direction of wall. Appears as part of a greater system of similarly oriented faults & fractures.
62712J1		122.9	173	67	176	20	524-526	Slicks & mullions-decent	Nice fault; can follow to base & top of wall. Fairly planar. Slicks & mullions agree.
62712K1		149.4	24	68	205	3	529	Big mullion	Beautiful conjugate faults 60 degrees apart. Both have subhorizontal slicks and mullions, and break out nicely. Faults merge at base where they meet; both continue above with slight change in orientation. Photos 527-530.
62712K2		149.7	175	57	359	4	530	Big mullion + slicks	
62712L1		153.4	7	79			531-532		Very distinct fault; traceable up and down. No kinematic indicators.
62712-1	East area, south side floor		344	60					1 & 2 appear to be conjugate faults
62712-2			205	54					
62712-3			352	64					Subhorizontal slicks? Not well defined
62712-4			326	71					In berm- followed on floor. Subvertical slicks? Could also be lines of water flow.
62712-5			330	65					In berm- followed on floor. Subvertical slicks? Could also be lines of water flow.
62712-6			333	72					
62712-7			339	73					
62812F1	"East wall" - north side 2nd bench	282.9	182	84	185	16	583-584	Decent mullion & ok slicks	Smallish fault with nicely defined plane. <1 cm separation. Extends up and down several meters but is not a dominant structure.
62812G1		291.2	315	78	308	5	586	Mullions-small, ok	
62812G2		291.2	302	77	304	6	587	Mullions & slicks - faint	G1 and G2 same strand; G2 1.5m below G1. Large scale mullions & sinuosity agree with measured value (roughly). Photos 585, 588.
62812H1		304.1	322	64	318	1	591	Mullions-good	H continues to top of wall with one step ~1m above measurements. Photos 589-590.
62812H2		304.1	312	77	318	11	592	Mulions-	

								good	
62812I1		329.8	186	53			595		No good kinematic indicators. Many subparallel planes- crumbly. Separation across I fault zone is 7 cm over several small steps.
62812J1		332.1	308	73	312	0	596	Nice mullions	Faults I & J appear to be a conjugate pair; neither offsets/separates the other, and they are at ~60 degrees to each other. Photos 593-595.
62812J2		332.1	314	75	316	3	597	Slicks- decent	~1m lower than J1, straight across from I1.
62812K1		371.9	191	74	12	3	600	Mullions- decent	2 cm separation, west side down.
62812L1		370.5, 371.9 (below)	222	11			601		Measurement taken with book extension.
62812L2			177	18			602		No good kinematic indicators on either plane of L. K and L1 intersect; L appears to break the plane surface of K, but no significant offset (<1cm). Photos 598-602.
62812M1		376.4, 380.5 (below)	106	15	173	12	603-606	Mullions- decent to good	Subvertical N intersects and subtly offsets M, which is lower angle. Face of N is cut; <1cm separation.
62812N1		378.8	13	68					No good kinematic indicators on N.
62812O1		395.2, 401.4	123	35	350	21	607-610	Good mullions	Fault O is low angle, well developed plane cut by high angle P. Offset of O by P creates large mullion consistent with other kinematic indicators. Several smaller faults make smaller mullions with similar orientation.
62812P1		396.9					608		P has poorly developed plane but offsets O by 1 cm, consistent with layers above & below. No good plane, but steep and dipping ~75
62812Q1		403.1, 408.4	110	24	171	22	611-614	Small mullions, decent	Another set of cross-cutting faults. Q is low angle; R higher angle with 2 strands that meet above Q; left side continues through Q but has no apparent offset.
62812R1		405.6	190	49					No good kinematic indicators.
62812S1	"East wall" - north side 2nd bench	413.9	318	82	317	6	617	Large, wavy mullions	Fault S is a major fault that extends to top & base of wall and breaks out easily. Lower angle T ends at S and does not cut surface. Photos 615-616.
62812T1		412.5, 413.9	17	9	333	5	618	Small mullions,	

								okay	
62812U1		425	135	90	136	26	619-622	Mullions & slicks - okay	Fault U is one of consistently trending significant faults that cuts to top of bench.
62812U2		425	142	88			619-622		Not great kinematic indicators.
62812V1		427.3	190	83	319	1	623-625	Mullions-better	Alternate & lower quality kinematic indicators (mullions) suggest 013/17. Mullions on V1 not great, seem to be incorrect w/ 28 cm west-down separation.
62812V2		427.3	~155	~89					Barely a plane. 10cm of west-down separation.
62812W1		432.1	321	83			626		Both faults W & X are dominant, throughgoing, breaking out faults that show no separation and possibly subhorizontal mullions.
62812X1	"East wall" - north side 2nd bench	437.3	319	80			626		
62812Y1		449.8	321	80			627		Similar to W and X; no visible kinematic indicators.
62812Z1		460	191	17	9	5	629		Fault Z is significant, throughgoing, and low angle. Fault system A is steeper and intersects Z. A1 (left) disappears in Z; A2 appears to be affected by Z: not offset, but plane is broken. Photo 628.
62812A1		460	345	78			630		No good indicators.
62812A2	"East wall" - 2nd bench corner	460	356	71			630		**Note: Corner of 2nd bench is pretty chopped up, with lots of loose/not in place blocks. No clean fault planes, but many big fractures.
62812B1		521, 524.5	340	56			631		Another large, traceable fault. No kinematic indicators.
62812C1		541.5	332	87			633		C1 & C2 parallel and similar orientation.
62812C2		544.5	331	82			634		
62812D1		541.5, 544.5	33	17			632-635		Fault D visibly cuts C1 & C2 planes, but no obvious separation. No discernible, consistent kinematic indicators on any plane. Photos 632-635.
62812E/1		554.1	223	27	268	22	636-637	Mullions & slicks - decent/good	E extends up and south to almost top of bench - can't tell because top is covered.
62812FF1	"East wall" - 2nd bench east side	565.2	228	26	346	26	638-641	Slicks	Reverse separation! 2cm vertical. More convinced of slicks after seeing this- could it be water flow?
62812GG1		577, 584	346	63	108	52	644	Mullions- ok	G & H are intersecting low angle faults (at least

62812HH1		579, 585	130	14	188	11	645	Mullions- ok	appear to be low angle cut as they are by plane of wall). Mullions just okay for both. Do not offset each other. Photos 642-645.
62812II1		590, 592.5	342	71	146	45	646-647	Mullions- ok/decent	Mullions could be a different feature.
62812JJ1		601, 602	57	18			648		Faults JJ, KK, LL are part of a system of similarly oriented throughgoing faults that break out with some difficulty and do not show separation or kinematic indicators.
62812KK1		615.4	61	23			649		
62812LL1		618.5	60	30			649		
62812MM1		621.5	91	29	150	28	650-651	Mullions & slicks - good	
62812NN1	"East wall" - 2nd bench east side	630.2, 635.5	344	70	115	59	653	Mullions - great	NN1 and NN2 are parallel/associated cracks. NN1 left; NN2 right. Photos 652-654.
62812NN2		630.2, 635.5	344	72	100	62	654	Mullions- great	
62812OO1		652.7, 655.2	264	21			655		Traceable several meters on wall; no visible kinematic indicators.
62812PP1		676.1, 679.2	252	23			656		Just a fracture? Extends several meters, though
62812QQ1		699.5, 701.8	242	24			657		Similar to OO and PP.
62812RR1		705.5, 708.2	329	63	129	25	659	Nice mullions	Faults RR & SS are close and similarly oriented. No visible separation, however. Photos 658-660.
62812SS1		710.8, 712.1	329	52	106	41	660	Nice mullions	
62812TT1		738.4, 740	223	10			661		No kinematic indicators.
62912U1	"East wall" - lower bench	458.5, 461.5	203	67	284	63	662-663	Slicks & mullions - okay	Traceable up wall several meters; covered above. Subvertical kinematic indicators- or water lines?
62912V1		490.5	87	28			665		On corner- affected by topography of terraces? Photos 664-666.
62912V2			102	29	160	25	665	Mullions- decent	
62912V3			107	32	135	19	666	Slicks- oxidized	
62912W1	NE corner - working from west to east		86	28	161	28	674	Mullions & slicks - good	
62912W2			82	33	160	33	675	Mullions & slicks - good	

62912X1			109	28	163	26	676	Mullions & slicks - good	Fault Y offsets fault X by 4 cm; Y does not reach W. Y and Z intersect but do not offset one another; however Z does break the face of Y. Photos 671-678.
62912Y1			27	37	172	24	677	Mullions - not great	
62912Z1			54	4	186	3	678	Slicks- okay	
62912A1			87	36	166	32	680	Mullions-good	Poor S/D measurements for B & C - too narrow to measure. Faults A, B, C appear to be part of a set. B&C merge to the west --> same fault? A splits into 2 strands about where B should intersect. Photos 679-682.
62912B1					162	16	681	Mullions-decent	
62912C1			~120	5	324	3	682	Mullions-okay/poor	
62912D1			79	29	148	25	683-684	Good mullions	
62912E/1			119	21	162	21	685-686	Slicks & mullions - good	
62912F1			106	30	163	24	685, 687	Slicks & mullions - good	
62912G1			210	22	346	20	688-689	Slicks- okay	Three faults east of G show 3-4 cm of west side down separation. Faults appear to dip steeply at 60 degrees or more; planes do not break out so I am unable to take measurements. Separation appears normal. Photos 690-694.
62912H1	NE corner - working from west to east		240	15			695-696		No consistent kinematic indicators.
62912I1			221	10	336	9	701	Slicks- okay	Faults H & I are same fault. Fault I cuts J, which is another high angle, normal separation fault (see photos 690-694). Separation 4 cm along I. J offsets dark layer 3 cm. Photos 697-699.
62912J1									High angle, normal separation.
62912K1			206	48			702		No good kinematic indicators. Traceable to top & base of bench wall.
62912L1			244	8			703		No good kinematic indicators.
62912M1			292	12	65	12	707	Mullions-okay	
62912N1			~horizontal	2	53	2	708-710	Lg mullions	Fault? Bedding plane? Both? Large scale waves (mullions?)

62912O1			173	52			711-712		No kinematic indicators, but this is a dominant fault. Whole wall breaks out along it.
62912P1			137	57			716		
62912P2			142	76	142	5	716	Left side mullions & slicks- faint/okay	P1 and P2 are relatively dominant faults.
62912Q1			148	75	151	8	717	Decent mullions	
62912R1	NE corner - working from west to east		332	28	66	28	718	Slicks- poor	
62912S1			334	83	335	50	718	Mullions- okay	Faults R & S merge to south just above measurements.
62912T1		402.8, 406.5	120	4	122	0	719-720	Slicks- okay/decent	Fault? Bedding plane? Conduit for meteoric water?
62912UU1		458.5, 461.5	139	14			721-724		
62912UU2		458.5, 461.5	256	26			721-724		
62912UU3		458.5, 461.5	166	18			721-724		
62912UU4		458.5, 461.5	193	19			721-724		
62912UU5		458.5, 461.5	342	63	73	56	724	Decent mullions	Many adjacent faults. 1 & 2 cross with no offset. Others are subparallel to 2. Photos 721-724.
62912VV1		490.5	280	28	1	24	725-727	Mullions- decent/okay	
62912WW1		495.2	220	20			725		No consistent indicators.
62912XX1		499.4	279	57	subvertical?		728-729		Beds separated 2 cm by X. Reverse? N side up. X separated 3 cm by Y; appears dextral.
62912YY1		500	205	5					No good indicators.
62912ZZ1		523.8	345	41	90	30	730-732	Slicks- okay	Silt 72 separated 6 cm (measured vertically); north side down.
62912AA1	East wall - lower bench (floor)	524.5, 528 (below)	180	15			733		No good indicators.
62912BB1		530.4	326	62	103	45	734-735	Decent mullions	No visible separation.

70112C1		539.9	197	15	306	13	768-769	Lg mullions & slicks - decent	Smaller fault but breaks out nicely. Does not extend much beyond excavated section.
70112D1		549.8, 553.0 (above)	330	68	108	53	770-771	Small mullions & slicks- decent	Also a smaller fault, but traceable at least 1 m above and less than 1 m below.
70112E/1		555.5, 557.5 (above)	346	42	91	41	772-773	Small mullions & slicks- decent	Similar to D.
70112F1		573	342	54			790		No consistent kinematic indicators.
70112F2		573	2	68	145	57	790	Mullions- decent/okay	
70112F3		573	6	67	155	50	791	Mullions & faint slicks - decent/okay	
70112F4		573	358	67	152	52	791	Mullions & faint slicks - decent/okay	Fault system F consists of many subparallel planes with generally similar kinematic indicators. Photos 789-791.
70112G1		597.2	260	10			792-793		Not convincingly a fault plane, but good plane. No kinematic indicators.
70112H1			220	27			794		
70212I		635, 637.5	147	26			798-799		Not convinced this is a fault. Fracture zone?
70212J		742.8	308	30	60	30	800-802	Slicks & mullions- good	3 cm separation on fault measured vertically. Breaks out with some difficulty.
70212K		894	282	85			803-804		Extends to top of wall; no good kinematic indicators.
70212L		677.4, 681.0	254	18	326	17	805-806	Slicks- okay	No apparent separation, but decent plane.
70212-1	Access road to lower east area, south wall		95	64					Large fractures along access road to lower east area. No kinematic indicators.
70212-2			104	65					
70212-3			104	65					
70212-4			93	64					
70212-5	Access road to east area, 2nd bench		102	55					Large fractures that generally extend to the base and top along 2nd bench access road to east area. No kinematic indicators and no visible separation.
70212-6			109	56					
70212-7			97	67					
70212-8			59	76					

70212-9			120	58					
70212-10			95	67					
70212-11			34	75					
70212-12			27	53					
70212-13			28	87					
70212-14			117	63					
70212-15			116	65					
70212-16			34	82					
70212-17			33	83					
70212-18			46	77					
70212-19			116	81					
70212-20	Lower east area		353	45	84	44	810	Slicks & mullions- decent/good	Fault near trench (southern notch). Peeled back layers from bottom to top (bottom 20, top 21). 6 cm separation, measured vertically, on S wall in trench. Photos 815-816.
70212-21			346	39	60	36	811-814	Slicks- decent	See above.
70212-22			352	60			817-819		Further north. Relatively significant fault extending meters to the south (up) and appears to sole into bedding to north (down)/steps onto another fault above with similar orientation.
70212-23			330	46			820-821		Further north. Significant fault with 22 cm vertical separation, N side down. Appears normal.
70212-24	East side, upper road with "no trucks" sign		182	61	342	31	829-832	Slicks- okay	Separates "6 inch ash" by ~20 cm or more. Damage zone of subparallel faults 20-30 cm on each side. West side down. Photos 829-832.
70212-25			176	55			833		Fault to east of previous (24) by ~25 m. Part of a set of subparallel faults on this wall. This fault above 6" ash.
70212-26	East side, upper road with "no trucks" sign, corner		192	54			834-835		Large fault that runs top to bottom.
70212-27			348	55	82	54	834-835	Slicks-decent	Surface of 26 broken by 27. Conjugate pair?
70212-28			194	54	8	11	836-837	Mullions- great	28 is to the left of 26 & 27 by ~10 m.
70212-29			125	45			838-839		~8 m left of Fault 27. Fault 28 is lower; 29 is higher. Faults or fractures?
70212-30			187	50			838-839		

83012A									Set of fissures filled with dark brown sediment ranging in size from silt to sand. Layering is parallel to edges of fissure. At top, crack diameter is 8-10 cm; splits into multiple cracks at depth with minimum diameter 5 mm-2 cm. Photos 274-276. No separation or offset. Fissure extends to top- younger than all diatomite.
83012B			348						Large fissure filled with dark brown mud to fine gravel; occasional diatomite entrained. Rare woody material (younger?). 1 cm or less apparent separation with west side down. Bedding within fissure is subvertical and parallel to sides of crack. Traced on floor, crack trends 348. Width 14 cm. Fissure extends to top. Photos 277-280.
83012C			129	69				left	C & D are a pair of intersecting faults with opposite separation: C shows 2 cm of west-down separation, and D has 2 cm of east-down separation. Both appear normal, forming somewhat of a miniature graben. Neither plane breaks out particularly well, and there are no visible kinematic indicators as a result.
83012D			2	36				right	
83012E			140	78				left	Steep fault with 11 cm of west down separation. Plane does not break out well, so there is greater uncertainty in measurement.
83012F			355	44				right	7 cm of east-down separation.
83012G	Straw area (south)							283-285	Another dark brown fissure, 1.5 cm wide. Cuts fault plane, so younger than fault. Extends to top. Fill is silt to fine gravel; majority is coarse sand.
83012H			152	55				286-287	Fault with 13 cm of west-down separation. No compelling kinematic indicators.
83012I	Straw area (south)							288-291	Fissure filled with diatomite- two dark layers above are unaffected. Cuts one dark layer- no separation other than opening of the crack. Crack width varies 5" to 8.5". Secondary fissure to left? (see photos). Or discoloration/differential fluid flow & oxidation?

83012J								292-294	Another large, dark brown fissure filled with silt - gravels. Runs subvertically to top of bench (surface?). Bedding also subvertical. Many associated fractures; main crack is more sinuous than others. Width 5.5 cm.
83012K			140	64				295-297	Fault part of system of cracks & faults surrounding fissure J. Steeply dipping with 6.5 cm of west-down separation.
83012L			160	49				300-302	Small fault (0.5 cm or less separation) exploited by fluids & roots. Breaks out nicely, but too many roots for reliable indicators.
83012M			161	43				308-309	Crack that extends to top of bench; exploited by fluids. Breaks out well. No separation.
83112N			156	38				310-311	Similar to L & M: crack with little to no separation, exploited/enhanced by fluids. This particular crack is part of system with almost 1 m of separation.
83112O			160	56				315	Crack similar to previous. No separation.
83112P			13	29				316	Crack similar to previous; no separation. * Compare this orientation to previous.
83112Q			356	~vertical				317-325	Huge sediment-filled crack/fissure. Many associated fluid-affected faults with separation. No separation on crack itself except for opening.
83112R			180	59				326-328	R & S are roughly parallel and part of the crack system associated with fissure Q. Separation along fault on wall surface: R- 23 inches; S- 9 inches. Both faults are west side down.
83112S			162	60				329-330	
83112T1			151	65			Subvertical small mullions		
83112T2			148	63					
83112T3			151	69					Numbered 1-4, starting at lower left and moving clockwise. System T has 25 inches of separation overall, all west side down. Extends to top & floor.
83112T4	Straw area (south)		149	60				331-333	

83112U			44	43				334-335	Fluid-affected crack, separation 3 cm vertically east side down. Fault extends to base and top of bench.
83112V			150	77				336-337	Major fault extending to base & top of bench. 11 cm of west-down separation.
83112W			0	50				338-339	17 inches of separation along fault, east side down. Fluid enchanced. Smooth fault plane surface, no kinematic indicators.
83112X			175	86				340-342	Fracture, no separation. Surface pink and hard-fluid deposits? Related to volcanics? Rocky's measurement 004/88.
83112Y	Straw area (south)		155	88					Complex and attractively patterned system of faults and fractures, many fluid-affected, with total separation of roughly 54 inches, measured vertically. Measured plane is only which breaks out at all, and does not do so well even so. ~20 inches of separation along measured plane, which greater than any other strand.

APPENDIX B

STEREONET GROUPINGS

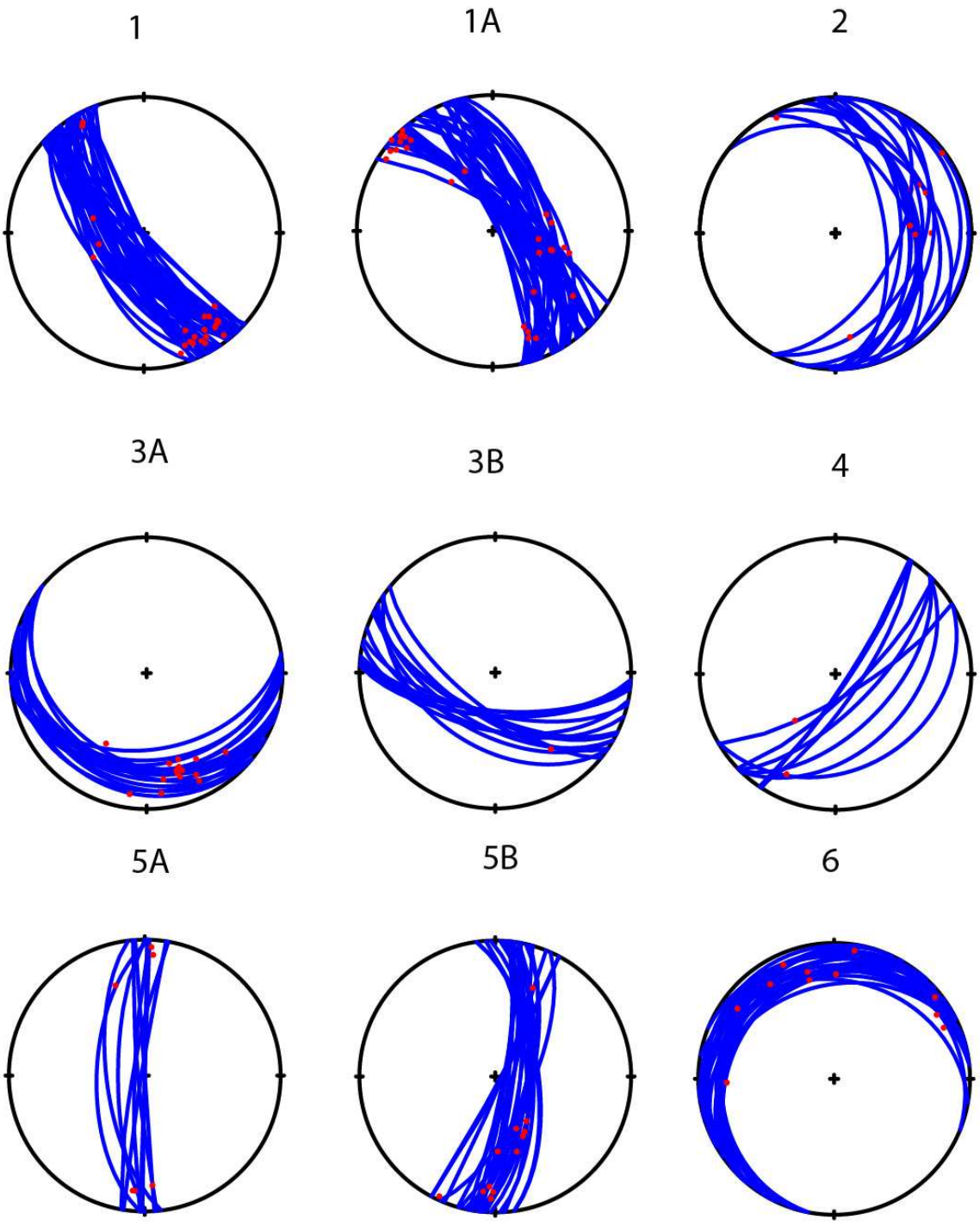

REFERENCES CITED

Dzurisin, D., Donnelly-Nolan, J.M., Evans, J.R., Walter, S.R., 1991. Crater subsidence, seismicity, and structure near Medicine Lake volcano, California. Journal of Geophysical Research 96, B10, 16,319-16,333.

Faulds, J.E., Henry, C.D., Hinz, N.H., 2005. Kinematics of the northern Walker Lane: An incipient transform fault along the Pacific-North American plate boundary. Geology 33, 6, 505-508.

Gardner, M.C., 1960. Geology of portions of the Bartle, Big Bend, Hambone, and Pondosa Quadrangles, California. Base map United State Geological Survey Quadrangle maps, scale 1:48,000.

Hammond, W.C., and Thatcher, W., 2005. Northwest Basin and Range tectonic deformation observed with the Global Positioning System, 1999-2003. Journal of Geophysical Research 110, B10405, doi:10.1029/2005JB003678.

Lahontan GeoScience, Inc., 2012, Seismogenic deformation in the Pit River region, Shasta County, California. October 2012. 1-40.

McCaffrey, R., 2005. Block kinematics of the Pacific-North America plate boundary in the southwestern United States from inversion of GPS, seismological, and geological data. Journal of Geophysical Research 110, B07401, doi:10.1029/2004JB003307.

McCaffrey, R., Qamar, A.I., King, R.W., Wells, R., Khazaradze, G., Williams, C.A., Stevens, C.W., Vollick, J.J., and Zwick, P.C., 2007. Fault locking, block rotation and crustal deformation in the Pacific Northwest. Geophysical Journal International 169, 1315-1340, doi:10.1111/j.1365-246X.2007.03371.x.

Miller, M.M., Johnson, D.J., Rubin, C.M., Dragert, H., Wang, K., Qamar, A., and Goldfinger, C., 2001. GPS-determination of along-strike variation in Cascadia margin kinematics: Implications for relative plate motion, subduction zone coupling, and permanent deformation. Tectonics 20, 2, 161-176.

Muffler, L.J.P., Clynne, M.A., and Champion, D.E., 1994. Late Quaternary normal faulting of the Hat Creek Basalt, northern California. GSA Bulletin 106, 195-200.

Muffler, L.P., Champion, D.E., Calvert, A.T., and Clynne, M.A., 2012. AGU Fall Meeting 2012. Poster V33B-2868.

Murray, M.H. and Lisowski, M., 2000. Strain accumulation along the Cascadia subduction zone. Geophysical Research Letters 27, 22, 3631-3634.

Norris, R.D., Meagher, K.L., Weaver, C.S., 1997. The 1936, 1945-1947, and 1950 earthquake sequences near Lassen Peak, California. Journal of Geophysical Research 102, B1, 449-457.

Poland, M., Burgmann, R., Dzurisin, D., Lisowski, M., Masterlark, T., Owen, S., Fink, J., 2006. Constraints on the mechanism of long-term, steady subsidence at Medicine Lake volcano, northern California, from GPS, leveling, and InSAR. Journal of Volcanology and Geothermal Research 150, 55-78.

Sawyer, T.L., 2010. Sierra Nevada-Cascade Range boundary zone, northeastern California- Newly recognized Quaternary structural boundary of the northern Sierra Nevada microplate. Geological Society of America Abstracts with Programs 42, 5, 134.

Sawyer, T.L., 2011. Quaternary Fault Activity Map. In: Piedmont Geosciences, Geologic Investigation of Fault 3432, Pit No.3 Dam Area. Scale 1:150,000.

Sawyer, T.L., Ramelli, A.R., 2012. Structural analysis, evaluation, and Quaternary activity of the Hat Creek and Rocky Ledge faults, Shasta County, northeastern California. Piedmont Geosciences report, October 2012, 1-42.

Turrin, B.D., Muffler, L.J.P., Clynne, M.A., and Champion, D.E., 2007. Robust 24±6 ka $^{40}Ar/^{39}Ar$ age of a low-potassium tholeiitic basalt in the Lassen region of NE California. Quaternary Research 68, 96-110.

Twiss, R.J. and Moores, E.M., 2007. Structural Geology, 2nd ed. W.H. Freeman, New York.

White, I.R. and Crider, J.G., 2006. Extensional fault-propagation folds: mechanical models and observations from the Modoc Plateau, northeastern California. Journal of Strucutral Geology 28, 1352-1370.